PHYSICAL REVIEW B **95**, 075135 (2017)

Topological semimetals protected by off-centered symmetries in nonsymmorphic crystals

Bohm-Jung Yang,[1,2,3] Troels Arnfred Bojesen,[4] Takahiro Morimoto,[5] and Akira Furusaki[4,6]

[1]*Department of Physics and Astronomy, Seoul National University, Seoul 08826, Korea*
[2]*Center for Correlated Electron Systems, Institute for Basic Science (IBS), Seoul 08826, Korea*
[3]*Center for Theoretical Physics (CTP), Seoul National University, Seoul 08826, Korea*
[4]*RIKEN Center for Emergent Matter Science, Wako, Saitama, 351-0198, Japan*
[5]*Department of Physics, University of California, Berkeley, California 94720, USA*
[6]*Condensed Matter Theory Laboratory, RIKEN, Wako, Saitama, 351-0198, Japan*

(Received 16 November 2016; revised manuscript received 26 January 2017; published 21 February 2017)

Topological semimetals have energy bands near the Fermi energy sticking together at isolated points/lines/planes in the momentum space, which are often accompanied by stable surface states and intriguing bulk topological responses. Although it has been known that certain crystalline symmetries play an important role in protecting band degeneracy, a general recipe for stabilizing the degeneracy, especially in the presence of spin-orbit coupling, is still lacking. Here we show that a class of novel topological semimetals with point/line nodes can emerge in the presence of *an off-centered rotation/mirror symmetry* whose symmetry line/plane is displaced from the center of other symmorphic symmetries in nonsymmorphic crystals. Due to the partial translation perpendicular to the rotation axis/mirror plane, an off-centered rotation/mirror symmetry always forces two energy bands to stick together and form a doublet pair in the relevant invariant line/plane in momentum space. Such a doublet pair provides a basic building block for emerging topological semimetals with point/line nodes in systems with strong spin-orbit coupling.

DOI: 10.1103/PhysRevB.95.075135

I. INTRODUCTION

Dirac particles with a pseudorelativistic energy dispersion have come to the fore in condensed matter physics research after the discovery of graphene [1]. To protect the fourfold degeneracy at a Dirac point in graphene, two conditions should be satisfied. One is the simultaneous presence of time-reversal (T) and inversion (P) symmetries, and the other is the absence of spin-orbit coupling. When these two conditions are satisfied at the same time, the Berry phase around a Dirac point has a quantized value of π, which guarantees the stability of the Dirac point.

Recently, there have been extensive efforts to extend the physics of the two-dimensional (2D) graphene to three-dimensional (3D) systems [2–19]. A natural starting point is to search for a 3D Dirac point protected by the PT symmetry and the associated π Berry phase. Interestingly, however, it is found that the PT symmetry protects a Dirac line node, instead of a Dirac point, which gives rise to a 3D semimetal with Dirac line nodes where fourfold band degeneracy occurs along a line in momentum space [2–10]. As in the case of graphene, such a Dirac line node protected by the PT symmetry is unstable in the presence of the spin-orbit coupling. It is also reported that a Dirac line node can exist in systems with a mirror symmetry when two bands with different mirror eigenvalues cross in the mirror plane [11–16]. However, the resulting line node is also unstable once the spin-orbit coupling is turned on.

In fact, the existence of a 3D Dirac point in systems with the spin-orbit coupling requires the introduction of additional crystalline symmetries other than the time-reversal and the inversion symmetries [20–26]. Up to now, two different recipes are known to yield 3D Dirac semimetals with point nodes. One is to introduce an additional uniaxial rotation symmetry where 3D Dirac points can occur when two bands with different rotation eigenvalues cross on the rotation axis [22–24]. Cd_3As_2 and Na_3Bi belong to this class [27–32]. Although a Dirac point does not carry a nonzero monopole charge which protects a Weyl point in the case of Weyl semimetals, the rotation symmetry provides an integer topological charge at the Dirac point, thus guarantees its stability [25].

The second recipe is to introduce an additional nonsymmorphic symmetry such as glide mirrors or screw rotations. When the double point group of a crystal possesses a four-dimensional irreducible representation, a Dirac point can appear at the Brillouin zone (BZ) boundary [20,21]. For several representative space groups, projective symmetry group analysis has been performed, which suggests β-BiO_2 [20] and distorted spinel compounds [21] as candidate systems of 3D Dirac semimetals belonging to this class. Since each Dirac point is protected by a different combination of crystalline symmetries depending on the space group of the crystal, careful symmetry analysis is required, case by case, to find the relevant topological charge of each Dirac point.

In this paper, we propose an alternative mechanism to realize novel 3D semimetals with Dirac point/line nodes in systems with strong spin-orbit coupling as well as P and T symmetries. To protect nodal points/lines with fourfold degeneracy, we find that *off-centered crystalline symmetries* play a crucial role. In contrast to the case of ordinary glide mirror or screw rotation symmetries having a partial translation in the invariant space of the associated point group symmetry, an *off-centered rotation/mirror* symmetry involves a partial translation that is orthogonal to the invariant space. In centrosymmetric crystals, such an off-centered symmetry naturally arises as a combination of a screw/glide symmetry and inversion symmetry P. An off-centered mirror/rotation symmetry possesses the characteristics of both the symmorphic and nonsymmorphic symmetries. Namely, it has momentum independent quantized eigenvalues, whereas its commutation relation with inversion symmetry P depends on

the momentum. Due to such a mixed nature of the off-centered symmetry, a pair of bands, each with Kramers degeneracy, form *a doublet pair* in its invariant space in the first BZ, and provide a basic building block for nodal points/lines. Similarly, when the rotation axis (mirror plane) of a screw (glide) symmetry does not pass the inversion center, an *off-centered screw (glide)* symmetry can be defined, which also leads to doublet pair formation and emerging Dirac points (lines) in the relevant invariant space. When an external magnetic field is applied to these semimetals, a Dirac-type point/line node with fourfold degeneracy splits into two Weyl-type point/line nodes with twofold degeneracy, with emergent surface states connecting the split nodes.

The rest of the paper is organized as follows. The nature of off-centered rotation/mirror symmetries is described in Sec. II. In Sec. III (Sec. IV), we explain the basic mechanism protecting point (line) nodes with fourfold degeneracy by off-centered rotation (mirror) symmetries. A simple tight-binding Hamiltonian describing various topological semimetals protected by off-centered symmetries is proposed in Sec. V. The influence of time-reversal breaking on the topological semimetals is described in Sec. VI, which is followed by the discussion in Sec. VII. Detailed information about the tight-binding Hamiltonian is given in Appendix A. The topological charges of various semimetal phases are defined in Appendix B. The stability of nodal and line nodes is further supported by the Clifford algebras approach described in Appendix C. In Appendix D, we perform a low-energy $\boldsymbol{k}\cdot\boldsymbol{p}$ Hamiltonian analysis. Finally, we explain the properties of semimetals protected by off-centered screw/glide symmetries in Appendix E.

II. NATURE OF OFF-CENTERED ROTATION/MIRROR SYMMETRIES

Generally, a nonsymmorphic symmetry element $\widetilde{g}=\{g|\boldsymbol{t}\}$ is composed of a point group symmetry operation g and a partial lattice translation $\boldsymbol{t}=\boldsymbol{t}_\perp+\boldsymbol{t}_\parallel$ where $\boldsymbol{t}_\parallel$ ($\boldsymbol{t}_\perp$) is the component invariant (variant) under the point symmetry operation g [33]. For instance, in the case of a nonsymmorphic mirror symmetry $\widetilde{M}=\{M|\boldsymbol{t}\}$, we have

$$M\boldsymbol{t}_\parallel=\boldsymbol{t}_\parallel,\quad M\boldsymbol{t}_\perp=-\boldsymbol{t}_\perp. \tag{1}$$

Since $M^2=-1$ ($M^2=+1$) for particles with a half-integer (integer) spin, when the nonsymmorphic mirror symmetry $\widetilde{M}=\{M|\boldsymbol{t}\}$ is operated twice, it should be an element of the lattice translation group, i.e., $\{M|\boldsymbol{t}\}^2=\{M^2|2\boldsymbol{t}_\parallel\}\in\mathbb{T}$, where $\mathbb{T}$ is the group of the pure lattice translation of a given crystal. Thus $2\boldsymbol{t}_\parallel$ should be a unit lattice translation in the mirror invariant plane whereas $\boldsymbol{t}_\perp$ is not influenced by the constraint above.

In fact, $\boldsymbol{t}_\perp$ is a fragile quantity whose value depends on the choice of the reference point of the point group symmetry operation. For instance, if the reference point for the point group symmetry operation is shifted by $\boldsymbol{d}=\boldsymbol{d}_\perp+\boldsymbol{d}_\parallel$, the nonsymmorphic mirror symmetry $\{M|\boldsymbol{t}\}$ also translates to $\{M|\boldsymbol{t}-2\boldsymbol{d}_\perp\}$. Thus by choosing $2\boldsymbol{d}_\perp=\boldsymbol{t}_\perp$, the perpendicular component of the partial translation can be erased. The resulting nonsymmorphic mirror symmetry is conventionally considered as the definition of a glide mirror symmetry $\widetilde{M}^\parallel\equiv\{M|\boldsymbol{t}_\parallel\}$.

However, $\boldsymbol{t}_\perp$ can also play a nontrivial role in the presence of an additional point group symmetry $\{g|\boldsymbol{t}'\}$ centered at a different reference point with $\boldsymbol{t}'_\perp\neq\boldsymbol{t}_\perp$ modulo unit lattice translation. For instance, one can choose the inversion center as the reference point of the point group symmetry, thus inversion is given by $\{P|\boldsymbol{0}\}$ whereas the nonsymmorphic mirror is $\{M|\boldsymbol{t}\}$. Here, the important point is that an additional shift of the reference point affects the form of the two operators simultaneously. Namely, under the shift of the reference point by $\boldsymbol{d}=\boldsymbol{d}_\perp+\boldsymbol{d}_\parallel$, the two symmetry operators transform as $\{M|\boldsymbol{t}\}\longrightarrow\{M|\boldsymbol{t}-2\boldsymbol{d}_\perp\}$ and $\{P|\boldsymbol{0}\}\longrightarrow\{P|-2\boldsymbol{d}_\perp-2\boldsymbol{d}_\parallel\}$, which indicates that even if $\boldsymbol{t}_\perp$ is subtracted from the nonsymmorphic mirror symmetry by choosing $2\boldsymbol{d}_\perp=\boldsymbol{t}_\perp$, it preserves its identity in conjunction with the inversion symmetry P. Therefore in systems with the inversion symmetry, an off-centered mirror symmetry, defined as

$$\widetilde{M}^\perp\equiv\{M|\boldsymbol{t}_\perp\}, \tag{2}$$

deserves a separate consideration.

An off-centered rotation symmetry can also be defined in a similar way. A generic nonsymmorphic rotation symmetry element $\widetilde{C}_n=\{C_n|\boldsymbol{t}\}$ ($n=2,3,4,6$) satisfies

$$C_n\boldsymbol{t}_\parallel=\boldsymbol{t}_\parallel,\quad C_n\boldsymbol{t}_\perp=\boldsymbol{t}'_\perp, \tag{3}$$

where C_n denotes the n-fold rotation symmetry and $\boldsymbol{t}'_\perp$ is a partial translation rotated by C_n satisfying $\boldsymbol{t}_\perp\cdot\boldsymbol{t}'_\perp=|\boldsymbol{t}_\perp|^2\cos\frac{2\pi}{n}$. Since C_n fulfills $C_n^n=-1$ ($C_n^n=+1$) for particles with a half-integer (integer) spin, a nonsymmorphic rotation symmetry $\{C_n|\boldsymbol{t}\}$ is under the following constraint, $\{C_n|\boldsymbol{t}\}^n=\{C_n^n|n\boldsymbol{t}_\parallel\}\in\mathbb{T}$, thus $\boldsymbol{t}_\parallel$ should have the form of $\boldsymbol{t}_\parallel=\frac{p}{n}\hat{a}_\parallel$ $p=0,1,...,n-1$, where $\hat{a}_\parallel$ is the unit translation along the rotation axis. Again, $\boldsymbol{t}_\perp$ is not constrained in this case.

If the reference point for the point group symmetry operation is shifted by $\boldsymbol{d}=\boldsymbol{d}_\perp+\boldsymbol{d}_\parallel$, the nonsymmorphic rotation symmetry $\{C_n|\boldsymbol{t}\}$ also transforms to $\{C_n|\boldsymbol{t}+C_n\boldsymbol{d}_\perp-\boldsymbol{d}_\perp\}$. Thus by choosing $\boldsymbol{d}_\perp$ to satisfy $\boldsymbol{t}_\perp=\boldsymbol{d}_\perp-C_n\boldsymbol{d}_\perp$, $\boldsymbol{t}_\perp$ can be removed, leading to a conventional screw rotation symmetry $\widetilde{C}_n^\parallel\equiv\{C_n|\boldsymbol{t}_\parallel\}$. However, in the presence of an additional point group symmetry centered at a different reference point, such as $\{P|\boldsymbol{0}\}$, an off-centered nonsymmorphic rotation symmetry

$$\widetilde{C}_n^\perp\equiv\{C_n|\boldsymbol{t}_\perp\} \tag{4}$$

can be defined, and the partial translation $\boldsymbol{t}_\perp$ can cause intriguing physical consequences as shown in the following.

III. POINT NODES PROTECTED BY OFF-CENTERED ROTATION SYMMETRIES

In electronic systems having both time-reversal and inversion symmetries, eigenstates are doubly degenerate at any momentum. Due to level repulsion between degenerate bands, accidental band degeneracy is lifted unless additional crystalline symmetry is supplemented [24]. Here we show that the presence of an off-centered symmetry creates symmetry-protected band degeneracy at the BZ boundary. For simplicity, let us first introduce an off-centered twofold rotation $\widetilde{C}_{2z}^\perp=\{C_{2z}|\frac{1}{2}\hat{x}+\frac{1}{2}\hat{y}\}$ to an orthorhombic crystal with T and P

symmetries. Here, $\hat{x}$, $\hat{y}$, and $\hat{z}$ denote the unit lattice vectors in the x, y, and z directions, respectively. To understand the origin of band degeneracy, let us examine how a spatial coordinate $\boldsymbol{r} = (x,y,z)$ transforms under $\widetilde{C}_{2z}^{\perp}$,

$$\widetilde{C}_{2z}^{\perp} : (x,y,z) \longrightarrow \left(-x+\frac{1}{2}, -y+\frac{1}{2}, z\right),$$
$$(\widetilde{C}_{2z}^{\perp})^2 : (x,y,z) \longrightarrow (x,y,z). \tag{5}$$

One can see that since $(\widetilde{C}_{2z}^{\perp})^2$ does not accompany a partial translation, it is actually equivalent to a symmorphic operation C_{2z}^2, which leads to $(\widetilde{C}_{2z}^{\perp})^2 = -1$ independent of the spatial coordinate. Thus, at the momentum $\boldsymbol{k}$ invariant under $\widetilde{C}_{2z}^{\perp}$, each band $|\Psi(\boldsymbol{k})\rangle$ can be labeled by the momentum independent $\widetilde{C}_{2z}^{\perp}$ eigenvalue $\pm i$, $\widetilde{C}_{2z}^{\perp}|\Psi_{\pm}(\boldsymbol{k})\rangle = \pm i|\Psi_{\pm}(\boldsymbol{k})\rangle$. Since the system is invariant under $\widetilde{C}_{2z}^{\perp}$ along the four lines $\boldsymbol{k}_1 = (0,0,k_z)$, $\boldsymbol{k}_2 = (\pi,0,k_z)$, $\boldsymbol{k}_3 = (0,\pi,k_z)$, $\boldsymbol{k}_4 = (\pi,\pi,k_z)$ with $k_z \in [-\pi,\pi]$, a state $|\Psi(\boldsymbol{k})\rangle$ on any of these lines carries a constant $\widetilde{C}_{2z}^{\perp}$ eigenvalue.

Now we consider the combined effect of P and $\widetilde{C}_{2z}^{\perp}$. From the combined transformations

$$P\widetilde{C}_{2z}^{\perp} : (x,y,z) \longrightarrow \left(x-\frac{1}{2}, y-\frac{1}{2}, -z\right),$$
$$\widetilde{C}_{2z}^{\perp}P : (x,y,z) \longrightarrow \left(x+\frac{1}{2}, y+\frac{1}{2}, -z\right), \tag{6}$$

we obtain

$$\widetilde{C}_{2z}^{\perp}P|\Psi(\boldsymbol{k})\rangle = e^{ik_x+ik_y}P\widetilde{C}_{2z}^{\perp}|\Psi(\boldsymbol{k})\rangle. \tag{7}$$

Thus along the two $\widetilde{C}_{2z}^{\perp}$ invariant lines $\boldsymbol{k}_2 = (\pi,0,k_z)$, $\boldsymbol{k}_3 = (0,\pi,k_z)$ with $k_z \in [-\pi,\pi]$, P and $\widetilde{C}_{2z}^{\perp}$ anticommute, i.e., $\{\widetilde{C}_{2z}^{\perp}, P\} = 0$. Moreover, since the time-reversal symmetry T commutes with both P and $\widetilde{C}_{2z}^{\perp}$, we obtain $\{\widetilde{C}_{2z}^{\perp}, PT\} = 0$, which gives rise to

$$\begin{aligned}\widetilde{C}_{2z}^{\perp}[PT|\Psi_{\pm}(\boldsymbol{k})\rangle] &= -PT[\widetilde{C}_{2z}^{\perp}|\Psi_{\pm}(\boldsymbol{k})\rangle] \\ &= -PT[\pm i|\Psi_{\pm}(\boldsymbol{k})\rangle] \\ &= \pm i\,PT|\Psi_{\pm}(\boldsymbol{k})\rangle. \end{aligned}\tag{8}$$

Thus $|\Psi_{\pm}(\boldsymbol{k})\rangle$ and $PT|\Psi_{\pm}(\boldsymbol{k})\rangle$, which are locally degenerate at the momentum $\boldsymbol{k}$, have the same $\widetilde{C}_{2z}^{\perp}$ eigenvalues of $\pm i$. Therefore when two degenerate bands having different $\widetilde{C}_{2z}^{\perp}$ eigenvalues cross, the resulting band crossing point is protected and forms a 3D Dirac point with fourfold degeneracy.

In fact, the anticommutation relation between P and $\widetilde{C}_{2z}^{\perp}$ puts a strong constraint on the band structure along the $\widetilde{C}_{2z}^{\perp}$ invariant axis. Considering

$$\begin{aligned}\widetilde{C}_{2z}^{\perp}[P|\Psi_{\pm}(\boldsymbol{k})\rangle] &= -P[\widetilde{C}_{2z}^{\perp}|\Psi_{\pm}(\boldsymbol{k})\rangle] \\ &= -P[\pm i|\Psi_{\pm}(\boldsymbol{k})\rangle] \\ &= \mp i\,P|\Psi_{\pm}(\boldsymbol{k})\rangle, \end{aligned}\tag{9}$$

one can find that two energetically degenerate states $|\Psi_{\pm}(\boldsymbol{k})\rangle$ and $P|\Psi_{\pm}(\boldsymbol{k})\rangle$, which are located at $\boldsymbol{k}$ and $-\boldsymbol{k}$, respectively, have the opposite $\widetilde{C}_{2z}^{\perp}$ eigenvalues. Let us recall that at each momentum $\boldsymbol{k}$, a Kramers pair should have the same $\widetilde{C}_{2z}^{\perp}$ eigenvalue. This means that on the $\widetilde{C}_{2z}^{\perp}$ invariant axis where

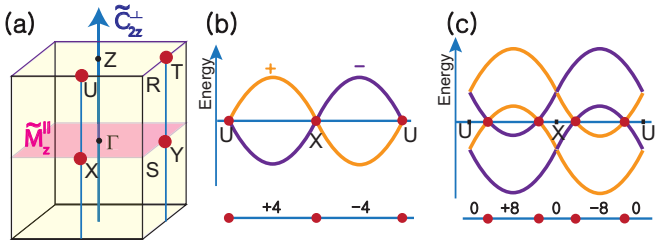

FIG. 1. 3D Dirac points protected by an off-centered twofold rotation $\widetilde{C}_{2z}^{\perp}$. (a) A schematic figure describing the distribution of 3D Dirac points in momentum space. The location of four 3D Dirac points is marked in red dots. The bold blue arrow indicates the axis for $\widetilde{C}_{2z}^{\perp}$ symmetry. The pink square indicates the plane of the glide mirror symmetry $\widetilde{M}_z^{\parallel}$, which is dual to $\widetilde{C}_{2z}^{\perp}$. (b) The band structure along the U-X-U line on which $\{P,\widetilde{C}_{2z}^{\perp}\} = 0$. A pair of degenerate bands (a doublet pair) form a 3D Dirac point at each time-reversal invariant momentum (TRIM). (c) The band structure when two doublet pairs cross on the U-X-U line. There are in total $4n$ (n is an integer) 3D Dirac points, which are all away from TRIMs. In (b) and (c), the integers in the bottom indicate the number $N(k_z)$ defined in Eq. (B2) from which the topological charge Q can be found by using Eq. (B1).

$\{P,\widetilde{C}_{2z}^{\perp}\} = 0$ is satisfied, there should be a pair of degenerate bands with different $\widetilde{C}_{2z}^{\perp}$ eigenvalues, which we call *a doublet pair*. Since a doublet pair should form a band structure which is symmetric with respect to a TRIM, they should be degenerate at the two TRIMs on the $\widetilde{C}_{2z}^{\perp}$ invariant axis as shown in Figs. 1(a) and 1(b). Here, each of the degenerate points with fourfold degeneracy represent a 3D Dirac point located at a TRIM.

Due to the presence of a quantized $\widetilde{C}_{2z}^{\perp}$ eigenvalue, the band crossing points between two different doublet pairs can also generate 3D Dirac points. Namely, as long as the two crossing bands have different $\widetilde{C}_{2z}^{\perp}$ eigenvalues, the crossing points are symmetry protected. In general, such a crossing between doublet pairs generates $4n$ (n is an integer) band crossing points, and the location of each Dirac point is away from TRIMs as shown in Fig. 1(c).

For comparison, let us consider a similar problem in systems with a twofold screw rotation $\widetilde{C}_{2z}^{\parallel} = \{C_{2z}|\frac{1}{2}\hat{z}\}$ satisfying

$$(\widetilde{C}_{2z}^{\parallel})^2 : (x,y,z) \longrightarrow (x,y,z+1). \tag{10}$$

Along the line invariant under $\widetilde{C}_{2z}^{\parallel}$, the relevant eigenstates satisfy $\widetilde{C}_{2z}^{\parallel}|\Psi_{\pm}(\boldsymbol{k})\rangle = \pm ie^{ik_z/2}|\Psi_{\pm}(\boldsymbol{k})\rangle$. Due to the momentum dependence of the eigenvalues, the two different $\widetilde{C}_{2z}^{\parallel}$ eigensectors should be interchanged when the momentum k_z is shifted by 2π. Moreover, it is straightforward to show that $\widetilde{C}_{2z}^{\parallel}P|\Psi(\boldsymbol{k})\rangle = e^{-ik_z}P\widetilde{C}_{2z}^{\parallel}|\Psi(\boldsymbol{k})\rangle$. Then along the line invariant under $\widetilde{C}_{2z}^{\parallel}$, where $\widetilde{C}_{2z}^{\parallel}|\Psi_{\pm}(\boldsymbol{k})\rangle = \pm ie^{\frac{i}{2}k_z}|\Psi_{\pm}(\boldsymbol{k})\rangle$, we obtain

$$\begin{aligned}\widetilde{C}_{2z}^{\parallel}[PT|\Psi_{\pm}(\boldsymbol{k})\rangle] &= e^{ik_z}PT[\widetilde{C}_{2z}^{\parallel}|\Psi_{\pm}(\boldsymbol{k})\rangle] \\ &= e^{ik_z}PT[\pm ie^{\frac{i}{2}k_z}|\Psi_{\pm}(\boldsymbol{k})\rangle] \\ &= \mp ie^{\frac{i}{2}k_z}PT|\Psi_{\pm}(\boldsymbol{k})\rangle, \end{aligned}\tag{11}$$

which show that the degenerate states $|\Psi_{\pm}(\boldsymbol{k})\rangle$ and $PT|\Psi_{\pm}(\boldsymbol{k})\rangle$ belong to different eigensectors of $\widetilde{C}_{2z}^{\parallel}$ symmetry. Therefore,

when two bands, each of which is doubly degenerate, touch, there always is some finite hybridization between degenerate bands. Thus $\widetilde{C}_{2z}^{\parallel}$ symmetry cannot protect a stable Dirac point at a generic momentum. One exception is when the band crossing happens at the time-reversal invariant momentum (TRIM) with $k_z = \pi$. In this case, two bands having the same $\widetilde{C}_{2z}^{\parallel}$ eigenvalues form a Kramers pair, and two Kramers pairs having different $\widetilde{C}_{2z}^{\parallel}$ eigenvalues are connected by P, leading to fourfold degeneracy [34]. However, such a degeneracy point does not form a 3D Dirac point. Instead, it becomes a part of a line node in the $k_z = \pi$ plane protected by $\widetilde{M}_z^{\perp} = \widetilde{C}_{2z}^{\parallel} P$, as discussed in Sec. IV.

IV. LINE NODES PROTECTED BY OFF-CENTERED MIRROR SYMMETRIES

An off-centered mirror symmetry can create a stable line node with fourfold degeneracy in systems with P and T symmetries. For convenience, let us consider $\widetilde{M}_x^{\perp} = \{M_x|\frac{1}{2}\hat{x}\}$, which transforms a spatial coordinate $\boldsymbol{r}$ in the following way:

$$\widetilde{M}_x^{\perp} : (x,y,z) \to \left(-x+\frac{1}{2},y,z\right),$$
$$(\widetilde{M}_x^{\perp})^2 : (x,y,z) \to (x,y,z). \tag{12}$$

From $M_x^2 = -1$, we obtain $(\widetilde{M}_x^{\perp})^2 = -1$ independent of a spatial coordinate. Thus, at the momentum $\boldsymbol{k}$ invariant under $\widetilde{M}_x^{\perp}$, i.e., at any momentum in the 2D plane with $k_x = 0$ or $k_x = \pi$, each band $|\Psi(\boldsymbol{k})\rangle$ can be labeled by the momentum independent $\widetilde{M}_x^{\perp}$ eigenvalue $\pm i$, i.e., $\widetilde{M}_x^{\perp}|\Psi_{\pm}(\boldsymbol{k})\rangle = \pm i|\Psi_{\pm}(\boldsymbol{k})\rangle$.

Now we consider the combined effect of P and $\widetilde{M}_x^{\perp}$. From

$$P\widetilde{M}_x^{\perp} :(x,y,z) \longrightarrow \left(x-\frac{1}{2},-y,-z\right),$$
$$\widetilde{M}_x^{\perp}P :(x,y,z) \longrightarrow \left(x+\frac{1}{2},-y,-z\right), \tag{13}$$

we obtain

$$\widetilde{M}_x^{\perp} P|\Psi(\boldsymbol{k})\rangle = e^{ik_x} P\widetilde{M}_x^{\perp}|\Psi(\boldsymbol{k})\rangle. \tag{14}$$

Thus in the $k_x = \pi$ plane, P and $\widetilde{M}_x^{\perp}$ anticommute, i.e., $\{\widetilde{M}_x^{\perp}, P\} = 0$. Moreover, since the time-reversal symmetry T commutes with both P and $\widetilde{M}_x^{\perp}$, we obtain $\{\widetilde{M}_x^{\perp}, PT\} = 0$, which gives rise to

$$\begin{aligned}\widetilde{M}_x^{\perp}[PT|\Psi_{\pm}(\boldsymbol{k})\rangle] &= -PT[\widetilde{M}_x^{\perp}|\Psi_{\pm}(\boldsymbol{k})\rangle] \\ &= -PT[\pm i|\Psi_{\pm}(\boldsymbol{k})\rangle] \\ &= \pm i\,PT|\Psi_{\pm}(\boldsymbol{k})\rangle. \end{aligned}\tag{15}$$

Thus $|\Psi_{\pm}(\boldsymbol{k})\rangle$ and $PT|\Psi_{\pm}(\boldsymbol{k})\rangle$, which are degenerate at the momentum $\boldsymbol{k}$, have the same $\widetilde{M}_x^{\perp}$ eigenvalues of $\pm i$. Therefore when two degenerate bands having different $\widetilde{M}_x^{\perp}$ eigenvalues cross, the resulting band crossing point is protected and forms a line node with fourfold degeneracy on the invariant plane $k_x = \pi$.

In fact, the anticommutation relation between P and $\widetilde{M}_x^{\perp}$ puts a strong constraint on the band structure in the $\widetilde{M}_x^{\perp}$ invariant plane. Considering

$$\begin{aligned}\widetilde{M}_x^{\perp}[P|\Psi_{\pm}(\boldsymbol{k})\rangle] &= -P[\widetilde{M}_x^{\perp}|\Psi_{\pm}(\boldsymbol{k})\rangle] \\ &= -P[\pm i|\Psi_{\pm}(\boldsymbol{k})\rangle] \\ &= \mp i\,P|\Psi_{\pm}(\boldsymbol{k})\rangle, \end{aligned}\tag{16}$$

we find that two energetically degenerate states $|\Psi_{\pm}(\boldsymbol{k})\rangle$ and $P|\Psi_{\pm}(\boldsymbol{k})\rangle$, which are located at $\boldsymbol{k}$ and $-\boldsymbol{k}$, respectively, have the opposite $\widetilde{M}_x^{\perp}$ eigenvalues. It is worth to remind that a Kramers pair at each momentum $\boldsymbol{k}$, which are degenerate due to PT symmetry, have the same $\widetilde{M}_x^{\perp}$ eigenvalue. This means that in the $k_x = \pi$ plane where $\{P, \widetilde{M}_x^{\perp}\} = 0$ is satisfied, two bands (each with Kramers degeneracy) having different $\widetilde{M}_x^{\perp}$ eigenvalues should form *a doublet pair* again as in the case of the off-centered rotation symmetry. Since the whole band structure in the $k_x = \pi$ plane is symmetric with respect to a TRIM, each doublet pair should be degenerate along a line, which passes two TRIMs as shown in Figs. 2(a) and 2(b). Here a set of the degenerate points form a line node with fourfold degeneracy.

Due to the presence of quantized $\widetilde{M}_x^{\perp}$ eigenvalues, a band crossing between two different doublet pairs can also generate nodal lines. Namely, as long as the two bands have different $\widetilde{M}_x^{\perp}$ eigenvalues, their crossing points are symmetry protected. In general, such crossing between two different doublet pairs generate $4n$ (n is an integer) nodal lines, and the location of each nodal line is away from TRIM as shown in Fig. 2(c).

For comparison, let us consider a similar problem in systems with a glide mirror $\widetilde{M}_x^{\parallel} = \{M_x|\frac{1}{2}\hat{y}+\frac{1}{2}\hat{z}\}$ satisfying

$$(\widetilde{M}_x^{\parallel})^2 :(x,y,z) \longrightarrow (x,y+1,z+1). \tag{17}$$

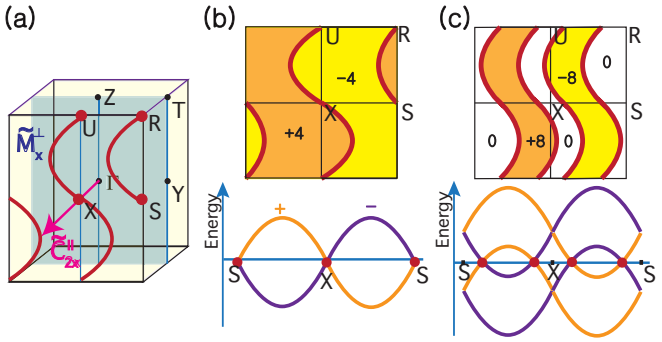

FIG. 2. 3D Dirac lines protected by an off-centered mirror symmetry $\widetilde{M}_x^{\perp}$. (a) A schematic figure describing the distribution of nodal lines in momentum space. The location of two line nodes in the $k_x = \pi$ plane is marked in red color. The blue square indicates the plane of the off-centered mirror symmetry $\widetilde{M}_x^{\perp}$. The bold pink arrow indicates the axis for the screw rotation $\widetilde{C}_{2x}^{\parallel}$ symmetry, which is dual to $\widetilde{M}_x^{\perp}$ symmetry. (b) Distribution of the integer $N(\pi,k_y,k_z)$ defined in Eq. (B9) in the $k_x = \pi$ plane from which the topological charge Q' of the line node can be computed by using Eq. (B8). The corresponding band structure along the S-X-S line is shown in the bottom. The doublet pair are degenerate at each TRIM, which is a part of line nodes in the $k_x = \pi$ plane. (c) Distribution of the integer $N(\pi,k_y,k_z)$, when two doublet pairs cross in the $k_x = \pi$ plane. There are in total $4n$ (n is an integer) nodal lines, which are away from TRIM. The corresponding band structure along the S-X-S line is shown in the bottom.

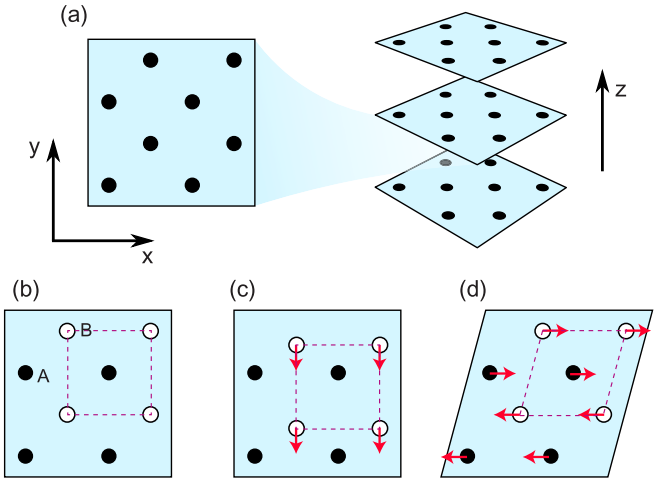

FIG. 3. Construction of 3D lattice models by stacking 2D layers. (a) A schematic figure describing a 3D lattice model obtained by vertical stacking of 2D square lattices. (b) Structure of a 2D layer where the B site in a unit cell is shifted along the z direction, thus the whole system has nonsymmorphic symmetries. (c) An additional shifting of B sites along the y direction, which breaks the symmetry $\widetilde{C}_{2z}^{\perp}$ (or equivalently, $\widetilde{M}_{z}^{\parallel}$). (d) An additional distortion of a unit cell, which breaks the symmetry $\widetilde{M}_{x}^{\perp}$ and $\widetilde{M}_{y}^{\perp}$ (or equivalently, $\widetilde{C}_{2x}^{\parallel}$ and $\widetilde{C}_{2y}^{\parallel}$).

In a plane invariant under $\widetilde{M}_{x}^{\parallel}$, the eigenstates satisfy $\widetilde{M}_{x}^{\parallel}|\Psi_{\pm}(\boldsymbol{k})\rangle = \pm i e^{\frac{i}{2}(k_y+k_z)}|\Psi_{\pm}(\boldsymbol{k})\rangle$. Due to the momentum dependence of the eigenvalues, the two different $\widetilde{M}_{x}^{\parallel}$ eigensectors should be interchanged when either k_y or k_z is shifted by 2π. Moreover, it is straightforward to show that

$$\widetilde{M}_{x}^{\parallel} P|\Psi(\boldsymbol{k})\rangle = e^{i(k_y+k_z)} P \widetilde{M}_{x}^{\parallel}|\Psi(\boldsymbol{k})\rangle. \tag{18}$$

Then in a 2D plane invariant under $\widetilde{M}_{x}^{\parallel}$, we obtain

$$\begin{aligned}\widetilde{M}_{x}^{\parallel}[PT|\Psi_{\pm}(\boldsymbol{k})\rangle] &= e^{-i(k_y+k_z)} PT[\widetilde{M}_{x}^{\parallel}|\Psi_{\pm}(\boldsymbol{k})\rangle] \\ &= \mp i e^{-\frac{i}{2}(k_y+k_z)} PT|\Psi_{\pm}(\boldsymbol{k})\rangle,\end{aligned} \tag{19}$$

which shows that $|\Psi_{\pm}(\boldsymbol{k})\rangle$ and $PT|\Psi_{\pm}(\boldsymbol{k})\rangle$, which are degenerate at the momentum $\boldsymbol{k}$, belong to different eigensectors of $\widetilde{M}_{x}^{\parallel}$ symmetry. This means that when two bands, each doubly degenerate due to the PT symmetry, overlap, there always is some finite hybridization between them at a generic momentum, thus a stable line node cannot be protected by $\widetilde{M}_{x}^{\parallel}$ symmetry in a mirror invariant plane. Instead, stable Dirac point nodes are protected by an off-centered symmetry $\widetilde{C}_{2x}^{\perp} = \widetilde{M}_{x}^{\parallel} P$ on its invariant lines $(k_x,\pi,0)$ and $(k_x,0,\pi)$.

V. MODEL

To demonstrate the general idea discussed up to now, we construct a 3D tight-binding Hamiltonian on a tetragonal lattice, which is composed of 2D square lattices stacked along the z direction as described in Fig. 3. For a 2D layer, we adopt the lattice model proposed in Ref. [34] in which a unit cell contains two sublattice sites, labeled A and B, where the B sublattice is displaced by $\boldsymbol{r}_{AB} = (\frac{1}{2},\frac{1}{2},\delta_z)$ $(0 < \delta_z < 1)$ from the A sublattice. Here we assume that both the in-plane and out-of-plane lattice constants to be unity. The vertical shift δ_z makes the symmetry of the lattice to be nonsymmorphic. Explicitly, the Hamiltonian in the real space is given by

$$\begin{aligned}\hat{H}^{(0)} = &\sum_{\langle i,j\rangle} t(\boldsymbol{r}_{ij})\hat{c}^{\dagger}_{\boldsymbol{r}_i}\hat{c}_{\boldsymbol{r}_j} + \sum_{\langle\langle i,j\rangle\rangle} t'(\boldsymbol{r}_{ij})\hat{c}^{\dagger}_{\boldsymbol{r}_i}\hat{c}_{\boldsymbol{r}_j} \\ &+ \sum_{\langle i,j,k\rangle} i\lambda(\boldsymbol{r}_{ij},\boldsymbol{r}_{jk})\hat{c}^{\dagger}_{\boldsymbol{r}_i}[(\boldsymbol{r}_{ij}\times\boldsymbol{r}_{jk})\cdot\boldsymbol{\sigma}]\hat{c}_{\boldsymbol{r}_k},\end{aligned} \tag{20}$$

where $t(\boldsymbol{r}_{ij})$ $[t'(\boldsymbol{r}_{ij})]$ is the hopping amplitude between same (different) sublattice sites, and $\lambda(\boldsymbol{r}_{ij},\boldsymbol{r}_{jk})$ denotes the spin-orbit induced hopping amplitude between the same sublattice sites i and k through the site j belonging to the other sublattice. Here, $\boldsymbol{r}_{ij} = \boldsymbol{r}_i - \boldsymbol{r}_j$ and the Pauli matrix $\boldsymbol{\sigma}$ indicates the spin degrees of freedom. More detailed information about the lattice model is given in Appendix A.

Let us note that $\hat{H}^{(0)}$ possesses not only the time-reversal symmetry T and the inversion symmetry P but also the off-centered symmetries $\widetilde{C}_{2z}^{\perp} = \{C_{2z}|\frac{1}{2}\hat{x}+\frac{1}{2}\hat{y}\}$, $\widetilde{M}_{x}^{\perp} = \{M_x|\frac{1}{2}\hat{x}\}$, and $\widetilde{M}_{y}^{\perp} = \{M_y|\frac{1}{2}\hat{y}\}$, thus the system corresponds to the space group No. 59. The corresponding screw/glide symmetries can be defined as $\widetilde{M}_{z}^{\parallel} = \widetilde{C}_{2z}^{\perp} P = \{M_z|\frac{1}{2}\hat{x}+\frac{1}{2}\hat{y}\}$, $\widetilde{C}_{2x}^{\parallel} = \widetilde{M}_{x}^{\perp} P = \{C_{2x}|\frac{1}{2}\hat{x}\}$, and $\widetilde{C}_{2y}^{\parallel} = \widetilde{M}_{y}^{\perp} P = \{C_{2y}|\frac{1}{2}\hat{y}\}$. By shifting the location of the B site relative to the A site in a unit cell, the symmetry of the Hamiltonian can be systematically lowered, thus one can examine the role of a particular symmetry to protect a relevant semimetal phase using a single lattice model.

First, we shift the position of the B site in a unit cell in the y direction, which makes $\boldsymbol{r}_{AB} = (\frac{1}{2},\delta_y \neq \frac{1}{2},\delta_z)$ as shown in Fig. 3(c). This distortion breaks $\widetilde{C}_{2z}^{\perp}$ and $\widetilde{M}_{y}^{\perp}$ symmetries, whereas $\widetilde{M}_{x}^{\perp}$ is preserved as well as the P and T symmetries, thus the system corresponds to the space group No. 11. The resulting band structure is shown in Fig. 4(a). One can clearly see that there are two line nodes in the $k_x = \pi$ plane, and each line node connects two TRIMs, which is consistent with the prediction of the general theory. To observe the band crossing between two doublet pairs described in Fig. 2(c), we construct an eight-band model by adding two copies of the 4×4 Hamiltonian in Eq. (20). As the hybridization between the two 4×4 blocks is turned on, each line node passing two TRIMs splits into two different nodal lines, thus one can observe four nodal lines, and none of them passes a TRIM as shown in Figs. 4(b) and 2(c).

The second distortion is achieved by deforming the lattice along the [110] direction, which breaks $\widetilde{M}_{x}^{\perp}$ and $\widetilde{M}_{y}^{\perp}$ symmetries whereas $\widetilde{C}_{2z}^{\perp}$ is preserved as well as the P and T symmetries, thus the system corresponds to the space group No. 13. [See Fig. 3(d).] As shown in Fig. 5(a), one can observe four Dirac points protected by $\widetilde{C}_{2z}^{\perp}$ symmetry located at TRIMs $\boldsymbol{k} = (\pi,0,0)$, $(\pi,0,\pi)$, $(0,\pi,0)$, and $(0,\pi,\pi)$. When the number of bands is doubled by combining two different 4×4 Hamiltonians, one can observe four Dirac points on the line $\boldsymbol{k} = (\pi,0,k_z)$ and also $\boldsymbol{k} = (0,\pi,k_z)$ with $k_z \in (-\pi,\pi)$, respectively, as shown in Fig. 5(b). Here none of Dirac points is located at a TRIM in agreement with the prediction of the general theory, and the relevant band structure is also consistent with Fig. 1(c).

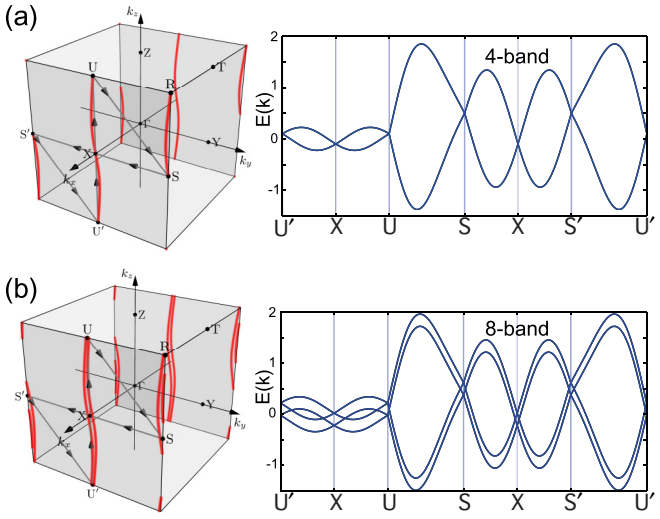

FIG. 4. Band structure of a semimetal with Dirac line nodes protected by $\widetilde{M}_x^{\perp} = \{M_x|\frac{1}{2}\hat{x}\}$ symmetry. (a) From four-band lattice models with P, T, and $\widetilde{M}_x^{\perp}$ symmetries. Here eigenstates are doubly degenerate at each momentum. Doublet pairs on the $k_x = \pi$ plane form two Dirac line nodes, each passes two TRIMs. The bold red lines in the left panel mark the points in the BZ where two bands stick together. (b) Similar plots from an eight-band lattice model. Crossing points between two doublet pairs form four Dirac line nodes on the $k_x = \pi$ plane, which correspond to those marked by red circles in Fig. 2(c). In the figures, U' and S' indicate the momenta equivalent to U and S, respectively.

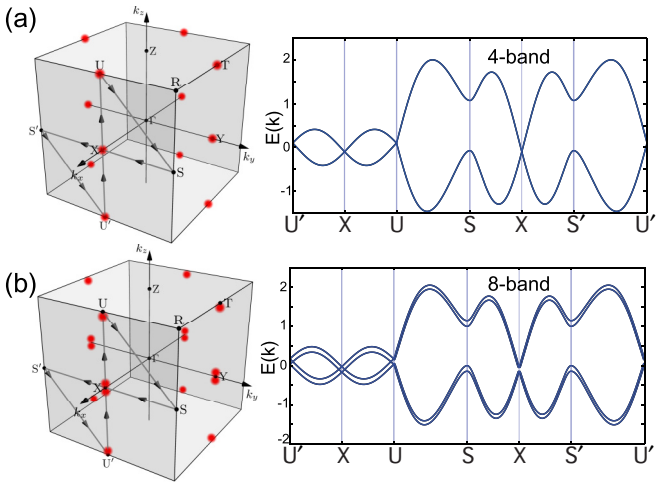

FIG. 5. Band structure of a semimetal with Dirac point nodes protected by $\widetilde{C}_{2z}^{\perp} = \{C_{2z}|\frac{1}{2}\hat{x} + \frac{1}{2}\hat{y}\}$ symmetry. (a) From four-band lattice models with P, T, and $\widetilde{C}_{2z}^{\perp}$ symmetries. Doublet pairs on the $\boldsymbol{k} = (\pi,0,k_z)$ and $\boldsymbol{k} = (0,\pi,k_z)$ lines with $k_z \in [-\pi,\pi]$, form Dirac point nodes at every TRIM. A bold red dot on the left marks the points where two bands stick together. (b) Similar plots from an eight-band lattice model. Crossing points between two doublet pairs form four Dirac points away from TRIM in both $\boldsymbol{k} = (\pi,0,k_z)$ and $\boldsymbol{k} = (0,\pi,k_z)$ lines with $k_z \in [-\pi,\pi]$, which correspond to those marked by red circles in Fig. 1(c). In the figures, U' and S' indicate the momenta equivalent to U and S, respectively.

VI. TIME-REVERSAL SYMMETRY BREAKING AND FERMI SURFACE TOPOLOGY

Since the stability of a Dirac point/line node requires the simultaneous presence of an off-centered symmetry ($\widetilde{M}_x^{\perp}$ or $\widetilde{C}_{2z}^{\perp}$) together with the T and P, it is interesting to examine the influence of symmetry breaking on the band structure. In particular, we find that the breaking of time reversal symmetry, due to Zeeman effect from external magnetic field ($\boldsymbol{H}$) or exchange coupling from doped magnetic ions, can create intriguing evolution in both the bulk and surface band structures, as summarized in Table I.

In the case of the semimetal with Dirac point nodes protected by $\widetilde{C}_{2z}^{\perp}$ symmetry, a Dirac point with fourfold degeneracy always splits into two Weyl points with twofold degeneracy [35,36], which accompanies a Fermi arc connecting the two Weyl points as shown in Fig. 6. More specifically, when $\boldsymbol{H} \parallel \hat{\boldsymbol{z}}$, the system preserves $\widetilde{C}_{2z}^{\perp}$ symmetry, and the two Weyl points split from a Dirac point is shifted along the k_z direction. On the other hand, when $\boldsymbol{H} \perp \hat{\boldsymbol{z}}$, the split Weyl points move in the plane normal to the k_z direction.

In the case of the semimetal with Dirac line nodes protected by $\widetilde{M}_x^{\perp}$ symmetry, the application of the external magnetic field causes more dramatic physical consequences. Firstly, when $\boldsymbol{H} \parallel \hat{\boldsymbol{x}}$, thus the system preserves $\widetilde{M}_x^{\perp}$ symmetry, a Dirac line node with fourfold degeneracy splits into two Weyl line nodes with twofold degeneracy as shown in Fig. 7. Here both the Dirac line node and the Weyl line nodes are located in the $k_x = \pi$ plane. Interestingly, the splitting of a Dirac line node is accompanied by emergent 2D surface states connecting the split Weyl line nodes, which originate from the π Berry phase around each Weyl line node [37–40]. The stability of the Weyl line node can be understood in the following way. Since $\widetilde{M}_x^{\perp}$ symmetry is preserved in the whole $k_x = \pi$ plane even in the presence of a magnetic field ($\boldsymbol{H} \parallel \hat{\boldsymbol{x}}$), each eigenstate still carries a quantized $\widetilde{M}_x^{\perp}$ eigenvalues of $\pm i$. Moreover, due to the inversion symmetry P satisfying $\{P,\widetilde{M}_x^{\perp}\} = 0$, if a state $|\Psi_{\pm}(\pi,k_y,k_z)\rangle$ at the momentum $\boldsymbol{k} = (\pi,k_y,k_z)$ has the $\widetilde{M}_x^{\perp}$ eigenvalues of $\pm i$, the state $|\Psi_{\pm}(\pi,-k_y,-k_z)\rangle \equiv P|\Psi_{\pm}(\pi,k_y,k_z)\rangle$ at the momentum $\boldsymbol{k} = (\pi,-k_y,-k_z)$ has the $\widetilde{M}_x^{\perp}$ eigenvalues of $\mp i$. Since the breaking of time-reversal symmetry splits each twofold degenerate band of zero field into two bands, the band structure has a configuration similar to the one shown in Fig. 2(c). Let us note that a TRIM is invariant under the inversion as well. Each state is nondegenerate at any $\boldsymbol{k}$ except at TRIMs due to the broken time-reversal symmetry. A stable Weyl line node with twofold degeneracy is formed as long as the degenerate states at the crossing point have different $\widetilde{M}_x^{\perp}$ eigenvalues.

When $\boldsymbol{H} \perp \hat{\boldsymbol{x}}$ breaks the $\widetilde{M}_x^{\perp}$ symmetry, a Dirac line node with fourfold degeneracy is lifted, and a band gap opens. Figure 7(c) shows the band structure when $\boldsymbol{H} \parallel \hat{\boldsymbol{z}}$. One can clearly see the opening of a band gap and the emergence of chiral surface modes near the U-X-U' line. In this case, for any 2D k_x-k_y plane with fixed k_z, the Chern number of the bands below the gap is equal to 1, and the system can be viewed as a 3D quantum Hall insulator having 2D chiral metallic states on the surface (provided that the Fermi energy is in the band gap). Therefore by changing the direction of the external magnetic field, one can introduce a transition from a semimetal with line

TABLE I. Fermi surface topology of the semimetals protected by off-centered symmetries in the presence/absence of magnetic field. We classify 3D topological semimetals with nodal point/lines protected by off-centered symmetries $\widetilde{C}_{2z}^{\perp}$, $\widetilde{M}_{x}^{\perp}$, $\widetilde{M}_{y}^{\perp}$ as well as time-reversal T and the inversion P symmetries in the presence/absence of external Zeeman fields. The "presence" or "absence" of each symmetry is indicated by "Yes" or "No," respectively, in the table. We note that the three off-centered symmetries are not independent due to the relation $\widetilde{C}_{2z}^{\perp} = \widetilde{M}_{y}^{\perp}\widetilde{M}_{x}^{\perp}$. Here a Dirac (Weyl) point/line node indicates a point/line node with fourfold (twofold) degeneracy.

Magnetic field ($\boldsymbol{H}$)	$\widetilde{C}_{2z}^{\perp}$	$\widetilde{M}_{x}^{\perp}$	$\widetilde{M}_{y}^{\perp}$	T	P	Fermi surface topology	Figures
$\boldsymbol{H}=0$	No	Yes	No	Yes	Yes	Dirac line node	4, 7(a)
$\boldsymbol{H}//[100]$	No	Yes	No	No	Yes	Weyl line nodes	7(b)
$\boldsymbol{H}//[010]$	No	No	No	No	Yes	Gapped	
$\boldsymbol{H}//[001]$	No	No	No	No	Yes	Gapped	7(c)
$\boldsymbol{H}=0$	Yes	No	No	Yes	Yes	Dirac point nodes	5, 6(a)
$\boldsymbol{H}//[100]$	No	No	No	No	Yes	Weyl point nodes	
$\boldsymbol{H}//[010]$	No	No	No	No	Yes	Weyl point nodes	
$\boldsymbol{H}//[001]$	Yes	No	No	No	Yes	Weyl point nodes	6(b)
$\boldsymbol{H}=0$	Yes	Yes	Yes	Yes	Yes	Dirac line nodes	8(a)–8(c)
$\boldsymbol{H}//[100]$	No	Yes	No	No	Yes	Weyl line nodes	8(d)–8(f)
$\boldsymbol{H}//[010]$	No	No	Yes	No	Yes	Weyl line nodes	
$\boldsymbol{H}//[001]$	Yes	No	No	No	Yes	Gapped	

nodes to a gapped phase, which can induce a dramatic change in the magneto-transport properties. All these results can also be confirmed by analyzing the low-energy $\boldsymbol{k}\cdot\boldsymbol{p}$ Hamiltonian as shown in detail in Appendix D.

Finally, when two off-centered symmetries $\widetilde{C}_{2z}^{\perp}$ and $\widetilde{M}_{x}^{\perp}$ exist at the same time, the system has an additional off-centered mirror symmetry $\widetilde{M}_{y}^{\perp}$ due to the relation $\widetilde{C}_{2z}^{\perp} = \widetilde{M}_{y}^{\perp}\widetilde{M}_{x}^{\perp}$. The presence of multiple crystalline symmetries leads to three Dirac line nodes at $\boldsymbol{k}=(\pi,0,k_z)$, $\boldsymbol{k}=(\pi,\pi,k_z)$, $\boldsymbol{k}=(0,\pi,k_z)$ with $k_z\in(-\pi,\pi)$, each of which is an open line parallel to the k_z direction as shown in Fig. 8. When the magnetic field $\boldsymbol{H}\parallel[100]$ or $\boldsymbol{H}\parallel[010]$ is applied to the system, one can find a semimetal with Weyl line nodes since at least one of the off-centered mirror symmetries is preserved in this case. One

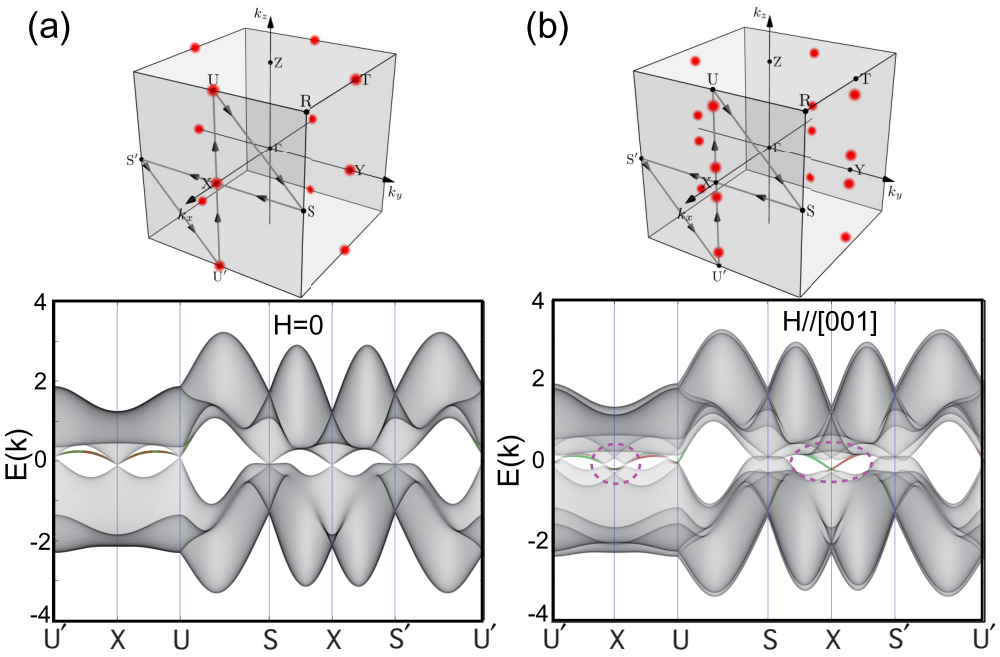

FIG. 6. Magnetic field induced transition of Dirac points into Weyl points. The bulk band structure of the four-band lattice model with P, T, and $\widetilde{C}_{2z}^{\perp}$ symmetries is shown in the lower panels after projection onto the surface BZ of a slab structure with a finite length L_x along the x direction. The states localized on the $x=0$ ($x=L_x$) surface are indicated by red (green) lines, respectively. (a) In the absence of magnetic field. There are four Dirac points at TRIMs (X, U, Y, and T) at $\boldsymbol{k}=(\pi,0,0)$, $(\pi,0,\pi)$, $(0,\pi,0)$, $(0,\pi,\pi)$, respectively. There are nontopological surface states on both surfaces which can be merged into bulk states through smooth deformation. (b) In the presence of magnetic field along the z direction ($h_z=0.2$). A Dirac point with fourfold degeneracy splits into two Weyl points, each with twofold degeneracy. Splitting of a Dirac point along the k_z direction accompanies emergent surface states (Fermi arcs) connecting two split Weyl points, which are marked with red dotted circles. In the figures, U' and S' indicate the momenta equivalent to U and S, respectively.

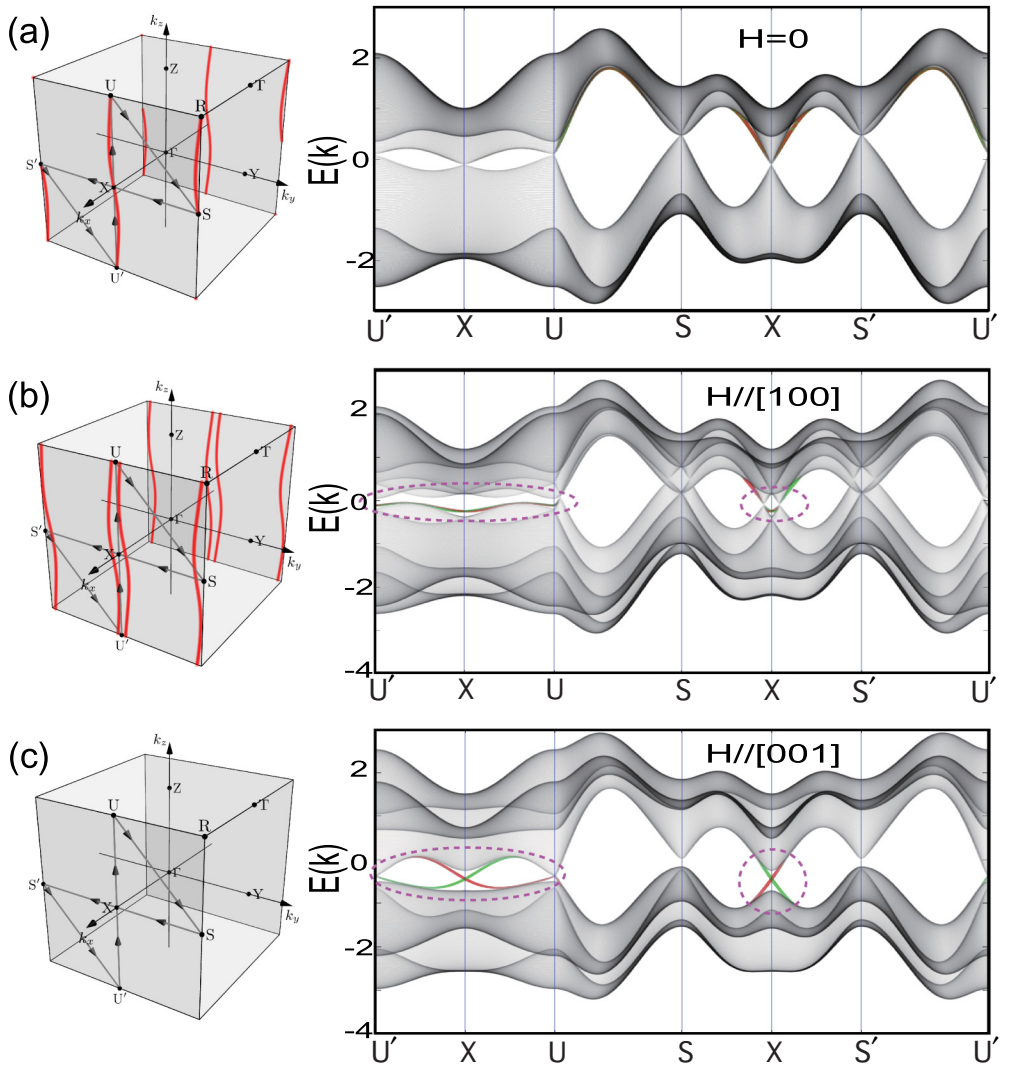

FIG. 7. Magnetic field induced transition of Dirac line nodes into Weyl line nodes and three-dimensional quantum Hall insulators. The bulk band structure of the four-band lattice model with P, T, and $\widetilde{M}_x^{\perp}$ symmetries is shown in the right panels after projection onto the surface Brillouin zone of a slab structure with a finite length L_x along the x direction. The states localized on the $x = 0$ ($x = L_x$) surface are indicated by red (green) lines, respectively. (a) In the absence of magnetic field. There are two Dirac line nodes on the $k_x = \pi$ plane. There are some nontopological surface states which can be merged with bulk states through smooth deformation. (b) In the presence of magnetic field along the x direction ($h_x = 0.3$). A Dirac line node with fourfold degeneracy splits into two Weyl line nodes, each with twofold degeneracy. Splitting of a Dirac line node accompanies emergent surface states connecting two split Weyl line nodes, which are marked with red dotted circles. (c) In the presence of magnetic field along the z direction ($h_z = 0.7$). A Dirac line node is fully gapped, and two-dimensional chiral surface states emerge, which are marked with red dotted circles. In the figures, U' and S' indicate the momenta equivalent to U and S, respectively.

the other hand, when $\boldsymbol{H} \parallel [001]$, thus both of the off-centered mirror symmetries are broken, a gapped insulator appears as summarized in Table I.

VII. DISCUSSION

In centrosymmetric crystals, an off-centered twofold rotation/mirror symmetry is obtained as a product of a glide mirror/twofold rotation and inversion P. Namely, $\widetilde{C}_2^{\perp} = \widetilde{M}^{\parallel} P$ and $\widetilde{M}^{\perp} = \widetilde{C}_2^{\parallel} P$. One can also ask about the role of other screw rotation symmetries $\widetilde{C}_{n,p}^{\parallel} = \{C_n | \frac{p}{n}\hat{a}_{\parallel}\}$ ($n = 3,4,6$ and $p = 0,1,\ldots,n-1$) combined with inversion. Since the invariant space of $\widetilde{C}_{n,p} P$ is just TRIMs on the rotation axis of $\widetilde{C}_{n,p}$, one can expect at most Dirac points on the rotation axis, which has already been extensively studied [24,25]. On the other hand, in the case of $\widetilde{C}_{4,p=1,3}^{\parallel}$ ($\widetilde{C}_{6,p=1,3,5}^{\parallel}$) symmetry which can generate twofold screw rotation $(\widetilde{C}_{4,p}^{\parallel})^2$ $((\widetilde{C}_{6,p}^{\parallel})^3)$ and the associated off-centered mirror $\widetilde{M}^{\perp}$, one may consider additional constraints on Dirac line nodes imposed by $\widetilde{C}_{4,p}^{\parallel}$ ($\widetilde{C}_{6,p}^{\parallel}$). It is straightforward to show that $\widetilde{C}_{4,p=1,3}^{\parallel}$ or $\widetilde{C}_{6,p=1,3,5}^{\parallel}$ does not commute with $\widetilde{M}^{\perp}$ in the mirror plane on the zone boundary where Dirac line nodes are expected, thus the screw rotation does not affect the distribution of $\widetilde{M}^{\perp}$ eigenvalues. One exception is the case with $\widetilde{C}_{6,3}^{\parallel}$ symmetry. Since $(\widetilde{C}_{6,3}^{\parallel})^2 = \{C_3|\mathbf{0}\}$ commutes with $\widetilde{M}^{\perp}$, the distribution

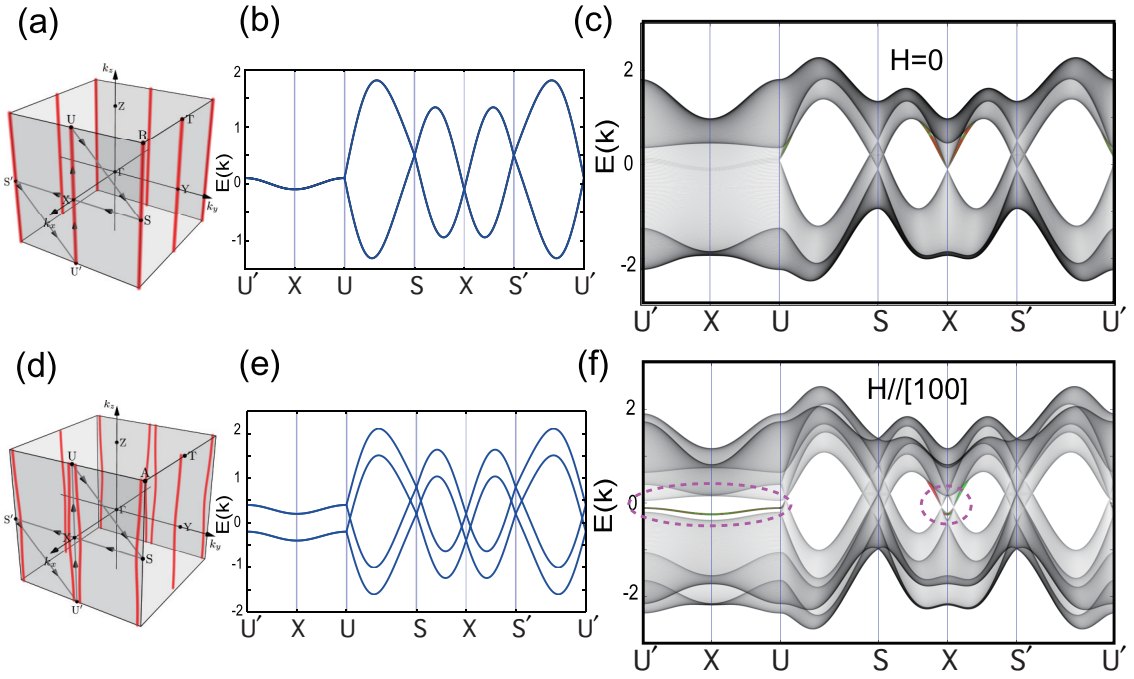

FIG. 8. Magnetic field induced transition of Dirac line nodes into Weyl line nodes in systems with both $\widetilde{M}_x^{\perp}$ and $\widetilde{C}_{2z}^{\perp}$. (a) In the absence of magnetic field. There are three open straight Dirac line nodes along $\boldsymbol{k} = (\pi,0,k_z)$, $(0,\pi,k_z)$ and (π,π,k_z) lines with $k_z \in [-\pi,\pi]$ due to the simultaneous presence of $\widetilde{M}_x^{\perp}$ and $\widetilde{M}_y^{\perp}$. (b) The bulk band structure of the four-band lattice model with P, T, $\widetilde{C}_{2z}^{\perp}$, and $\widetilde{M}_x^{\perp}$ symmetries. (c) The band structure of the slab structure with a finite length along the x direction are shown. The states localized on the $x = 0$ ($x = L_x$) surface are indicated by red (green) lines, respectively. (d)–(f) Similar plots in the presence of magnetic field along the x direction ($h_x = 0.3$). A Dirac line node with fourfold degeneracy splits into two Weyl line nodes, each with twofold degeneracy. Splitting of a Dirac line node accompanies emergent surface states connecting two split Weyl line nodes, which are marked with dotted circles. In the figures, U' and S' indicate the momenta equivalent to U and S, respectively.

of $\widetilde{M}^{\perp}$ also satisfies threefold rotation symmetry, which constrains the number of open line nodes to be a multiple of 3.

It is worth to note that the presence of inversion symmetry is not necessary to have off-centered symmetries. Off-centered symmetries can exist, in general, as long as a nonsymmorphic crystal with screw/glide symmetries contain an additional point group symmetry such as mirror symmetry whose reference point does not coincide with that of screw/glide symmetries. In noncentrosymmetric systems, stable Weyl point/line nodes with twofold degeneracy can be protected by off-centered symmetry when two bands with different eigenvalues cross in the relevant invariant space.

Up to now, we have considered $\boldsymbol{t}_{\perp}$ and $\boldsymbol{t}_{\parallel}$ separately. However, in many nonsymmorphic crystals, $\boldsymbol{t}_{\perp}$ and $\boldsymbol{t}_{\parallel}$ coexist, which gives rise to *off-centered screw/glide symmetries*. Interestingly, the off-centered twofold screw/glide symmetry can protect a single point/line node with fourfold degeneracy in an invariant space. For instance, let us consider a system corresponding to the space group No. 14 containing T, $\{P|\boldsymbol{0}\}$, and an off-centered glide mirror $\widetilde{M}_z^{\parallel,\perp} = \{M_z|\frac{1}{2}\hat{x} + \frac{1}{2}\hat{z}\}$ with $\boldsymbol{t}_{\perp} = \frac{1}{2}\hat{z}$ and $\boldsymbol{t}_{\parallel} = \frac{1}{2}\hat{x}$. On the $k_z = \pi$ plane, the Kramers degenerate $\widetilde{M}_z^{\parallel,\perp}$ eigenstates at each momentum have the same $\widetilde{M}_z^{\parallel,\perp}$ eigenvalues $\pm i e^{i\frac{1}{2}k_x}$. However, due to their momentum dependence, when k_x is shifted by 2π, two different $\widetilde{M}_z^{\parallel,\perp}$ eigensectors should be interchanged. This naturally gives rise to an open line node connecting two TRIMs at $\boldsymbol{k} = (0,0,\pi)$ and $(0,\pi,\pi)$ as shown in Figs. 9(d)–9(f). Contrary to the semimetal protected by $\widetilde{M}_x^{\perp}$ with an even number of nodal lines, the semimetal protected by the off-centered glide mirror $\widetilde{M}_z^{\parallel,\perp}$ has a single nodal line. This is because, due to the k_x dependence of $\widetilde{M}_z^{\parallel,\perp}$ eigenvalues, it is possible to get around the doubling in the number of line nodes [25]. (See Appendix E.) Repeating a similar analysis, one can easily see that an off-centered twofold screw rotation, $\widetilde{C}_{2z}^{\parallel,\perp} = \widetilde{M}_z^{\parallel,\perp} P = \{C_{2z}|\frac{1}{2}\hat{x} + \frac{1}{2}\hat{z}\}$, has momentum-dependent eigenvalues, which can give rise to a semimetal with a single Dirac point on each rotation axis. [See Figs. 9(a)–9(c).]

Let us note that a line node semimetal protected by an off-centered glide mirror is already discussed in Ref. [41]. Although the key role of an off-centered glide mirror on the protection of a nodal line with fourfold degeneracy is correctly described in this work, a line node predicted in Ref. [41] forms a closed loop, which is not consistent with our theory. We believe that a nodal line protected by a single off-centered glide mirror should have an open shape. Correct description of the shape of nodal lines is important to resolve the controversies related with the mechanism protecting the circular Dirac line node in $SrIrO_3$. To explain the origin of the Dirac line node in $SrIrO_3$, several different ideas are proposed including off-centered glide mirror symmetry [41], simultaneous presence of mirror and chiral symmetries [17], the presence of multiple nonsymmorphic symmetries [42].

TABLE II. Properties of candidate systems having Dirac line nodes with four-fold degeneracy in the presence of strong spin-orbit coupling. We show the shape/number of Dirac line nodes, and the associated symmetries in two candidate materials BaTaS [45], $SrIrO_3$ [42], and the model Hamiltonian $\hat{H}^{(0)}$ in Eq. (20) with/without the distortion described by $\hat{H}^{(1)}$ in Eq. (A2). These are the only examples proposed up to now which can support stable Dirac line nodes with four-fold degeneracy even in the presence of strong spin-orbit coupling. Here the number of line nodes indicates the minimal number of Dirac line nodes appearing near the Fermi level in each system when the nodal lines are assumed to be almost dispersionless.

Candidate system	Space group	Relevant symmetry	Shape of line nodes	Number of line nodes
$\hat{H}^{(0)}$	59	$\widetilde{M}_x^{\perp}$ or $\widetilde{M}_y^{\perp}$	open straight	2
$\hat{H}^{(0)}+\delta H^{(1)}(\boldsymbol{k})$	11	$\widetilde{M}_x^{\perp}$	open	1
BaTaS	194	$\widetilde{M}_z^{\perp}$	open straight	3
$SrIrO_3$	62	$\widetilde{C}_{2z}^{\parallel,\perp}$ and $\widetilde{C}_{2y}^{\parallel}$	closed loop	1

According to our theoretical analysis, the presence of a single nonsymmorphic symmetry can protect only line nodes with open shape. The presence of multiple nonsymmorphic symmetries is necessary to describe the circular nodal line in $SrIrO_3$ as proposed in Ref. [42]. More explicitly, in the presence of both n-glide and b-glide symmetries, four bands, each of which is doubly degenerate, should be coupled in the Brilouin zone [42,43], and a circular Dirac line node appears between the second and the third bands. This can be contrasted to the case with a single off-centered symmetry in which only two degenerate bands are coupled. In $SrIrO_3$, the line node is located in a 2D plane invariant under n-glide symmetry between two bands having different n-glide eigenvalues. Thus the band degeneracy along the line node can be maintained as along as n-glide symmetry is preserved, even when b-glide symmetry is broken as discussed in Ref. [44]. However, in the absence of b-glide symmetry, since four doubly degenerate bands are not necessarily entangled, they can be decoupled into two groups of bands, which accompanies the degeneracy lifting along the circular line node. Namely, the line node is not topologically stable any more, thus it can be removed via continuous deformation of the band structure.

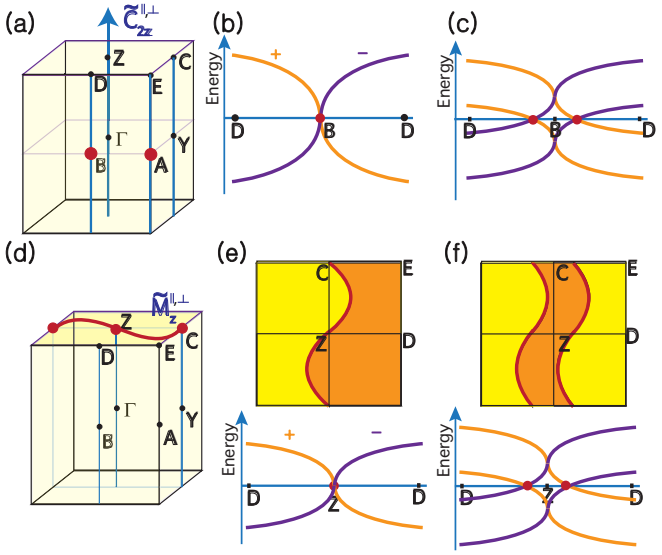

FIG. 9. Dirac points/lines protected by off-centered screw/glide symmetries. (a)–(c) Dirac points protected by off-centered twofold screw rotation $\widetilde{C}_{2z}^{\parallel,\perp}=\{C_{2z}|\frac{1}{2}\hat{x}+\frac{1}{2}\hat{z}\}$. (a) A schematic figure describing the distribution of 3D Dirac points in momentum space. The location of two 3D Dirac points is marked in red dots. Here high-symmetry momenta are labeled as in Ref. [33]. (b) The band structure along the D-B-D line on which $\{P,\widetilde{C}_{2z}^{\parallel,\perp}\}=0$. A pair of degenerate bands (a doublet pair) form a single 3D Dirac point at the time-reversal invariant momentum (TRIM) with $k_z=0$. (c) The band structure when two doublet pairs cross on the D-B-D line. There are in total $2n$ (n is an integer) 3D Dirac points, which are all away from TRIMs. (d)–(f) Dirac lines protected by off-centered glide mirror $\widetilde{M}_z^{\parallel,\perp}=\{M_z|\frac{1}{2}\hat{x}+\frac{1}{2}\hat{z}\}$. (d) A schematic figure describing the location of the nodal line in momentum space. The location of the line node in the $k_z=\pi$ plane is marked in red color. (e) Shape of a nodal line in the $k_z=\pi$ plane in which $\{P,\widetilde{M}_z^{\parallel,\perp}\}=0$ is satisfied. The corresponding band structure along the D-Z-D line is shown in the bottom. The doublet pair are degenerate at two TRIMs (C and Z points), which are a part of line nodes in the $k_z=\pi$ plane. (f) Shape of nodal lines when two doublet pairs cross in the $k_z=\pi$ plane. The corresponding band structure along the D-Z-D line is shown in the bottom.

$BaTaS_3$ is another material, which has stable Dirac line nodes with fourfold degeneracy in the presence of spin-orbit coupling. Interestingly, according to a recent first-principles calculation [45], it is found that the nodal lines in this material have open shape, which is consistent with our model calculation shown in Fig. 2(b). In this system, due to the additional mirror symmetry whose invariant plane is orthogonal to that of the off-centered mirror symmetry, the nodal lines have open shape similar to the case shown in Fig. 8(a). Though the role of the additional mirror symmetry is emphasized in Ref. [45], based on our theoretical consideration, we think that the presence of P, T, and an off-centered mirror is sufficient for the protection of the Dirac line node itself.

Table II summarizes the space group, relevant symmetry, and the shape of line nodes for the above two candidate materials and our model Hamiltonian. To sum up, we propose a general theoretical framework to understand a class of 3D semimetals with Dirac line/point nodes with fourfold degeneracy, which are stable in the presence of strong spin-orbit coupling. We have identified the presence of *off-centered crystalline symmetries* as a mechanism for the protection of the point/line nodes. Interestingly, in a recent work, it is found that off-centered crystalline symmetries can also protect band degeneracy in 2D semimetals [46], which shows that off-centered crystalline symmetries play a crucial role to protect a wide class of semimetals both in 2D and 3D.

According to our theoretical study, if the crystalline symmetries relevant to the protection of each nodal semimetal

is partially lifted by applying external magnetic field or doping magnetic ions, one can observe a significant change of Fermi surface topology, involved with the emerging topological semimetals with Weyl point nodes or Weyl line nodes, or even a gapped insulator. Such a tunability of the Fermi surface topology under magnetic field can provide a promising venue for various intriguing topological magneto-transport phenomena. Moreover, since both weak disorder (Coulomb potential) is irrelevant (marginally irrelevant) perturbation, the prediction based on noninteracting semimetals is perturbatively valid even in disordered (interacting) systems [47,48]. To understand the role of strong electron correlation and disorder, and, in particular, the combined effect of them are important issues to be studied in future research. For instance, a recent theoretical proposal for a possible spin liquid state with a nodal line [49] indicates that strong electron correlation can generate a variety of exotic topological phases with point/line nodes which are unexplored up to now.

ACKNOWLEDGMENTS

We are grateful to Robert-Jan Slager for useful comments. B.-J.Y was supported by IBS-R009-D1, Research Resettlement Fund for the new faculty of Seoul National University, and Basic Science Research Program through the National Research Foundation of Korea (NRF) funded by the Ministry of Education (Grant No. 0426-20150011). T.M. was supported by the EPiQS initiative of the Gordon and Betty Moore Foundation. A.F. was supported by JSPS KAKENHI Grant (No. 15K05141).

B.-J. Yang and T. A. Bojesen contributed equally to this work.

APPENDIX A: LATTICE MODEL

In the momentum space, the tight-binding Hamiltonian in Eq. (20) can be written as $\hat{H}^{(0)} = \sum_{\boldsymbol{k}} \hat{c}^{\dagger}(\boldsymbol{k}) H^{(0)}(\boldsymbol{k}) \hat{c}(\boldsymbol{k})$ with

$$\begin{aligned} H^{(0)}(\boldsymbol{k}) = &- [(t_1 + t_2 \cos k_z)\tau_x + t_2 \sin k_z \tau_y] \cos\frac{k_x}{2} \cos\frac{k_y}{2} \\ &- t_3(\cos k_x + \cos k_y) - t_4 \cos k_z \\ &+ (\lambda_1 - \lambda_2 \cos k_z)(\sin k_x \sigma_y - \sin k_y \sigma_x)\tau_z, \end{aligned} \tag{A1}$$

where the Pauli matrices $\tau_{x,y,z}$ denote the sublattice degrees of freedom. $\hat{H}^{(0)}$ is invariant not only under the time-reversal symmetry T and the inversion symmetry P but also under the off-centered symmetries $\widetilde{C}_{2z}^{\perp} = \{C_{2z}|\frac{1}{2}\hat{x} + \frac{1}{2}\hat{y}\}$, $\widetilde{M}_x^{\perp} = \{M_x|\frac{1}{2}\hat{x}\}$, and $\widetilde{M}_y^{\perp} = \{M_y|\frac{1}{2}\hat{y}\}$. At the Γ point, the symmetry operators are written as $T = i\sigma_y\mathcal{K}$, $P = \tau_x$, $\widetilde{C}_{2z}^{\perp} = i\sigma_z$, $\widetilde{M}_x^{\perp} = i\sigma_x$, and $\widetilde{M}_y^{\perp} = i\sigma_y$, where $\mathcal{K}$ is complex conjugation operator.

To understand the role of each off-centered symmetry, we distort the lattice in two different ways. First, we shift the position of the B site in a unit cell in the y direction, which makes $\boldsymbol{r}_{AB} = (\frac{1}{2}, \delta_y \neq \frac{1}{2}, \delta_z)$. This distortion breaks $\widetilde{C}_{2z}^{\perp}$ and $\widetilde{M}_y^{\perp}$ symmetries, and generates the following additional terms in the Hamiltonian:

$$\begin{aligned} \delta H^{(1)}(\boldsymbol{k}) = &[(t_1' + t_2' \cos k_z)\tau_y - t_2' \sin k_z \tau_x] \cos\frac{k_x}{2} \sin\frac{k_y}{2} \\ &+ (\lambda_1' - \lambda_2' \cos k_z) \sin k_x \sigma_z \tau_z \\ &- [\lambda_2'(\cos k_x + \cos k_y) + \lambda_3] \sin k_z \sigma_x \tau_z. \end{aligned} \tag{A2}$$

The full Hamiltonian $H^{(0)}(\boldsymbol{k}) + \delta H^{(1)}(\boldsymbol{k})$ supports nodal lines in the $k_x = \pi$ plane protected by the $\widetilde{M}_x^{\perp}$ symmetry. The 8×8 Hamiltonian with the band structure shown in Fig. 4(b) is given by $[H^{(0)}(\boldsymbol{k}) + \delta H^{(1)}(\boldsymbol{k})]\upsilon_0 + \lambda_4 \sigma_x \upsilon_y$, where υ_0 is a 2×2 unit matrix and $\upsilon_{x,y,z}$ are Pauli matrices in the new grading.

The second distortion is achieved by deforming the lattice along the [110] direction, which breaks $\widetilde{M}_x^{\perp}$, $\widetilde{M}_y^{\perp}$ symmetries and generates the following term,

$$\begin{aligned} \delta H^{(2)}(\boldsymbol{k}) = &- [(t_1' + t_2' \cos k_z)\tau_x + t_2' \sin k_z \tau_y] \sin\frac{k_x}{2} \sin\frac{k_y}{2} \\ &- (\lambda_1' + \lambda_2' \cos k_z)(\sin k_x \sigma_x - \sin k_y \sigma_y)\tau_z \\ &+ \lambda_2' \sin k_z (\cos k_x - \cos k_y)\sigma_z \tau_z. \end{aligned} \tag{A3}$$

The full Hamiltonian $H^{(0)}(\boldsymbol{k}) + \delta H^{(2)}(\boldsymbol{k})$ supports nodal points protected by the $\widetilde{C}_{2z}^{\perp}$ symmetry. The 8×8 Hamiltonian with the band structure shown in Fig. 5(b) is given by $[H^{(0)}(\boldsymbol{k}) + \delta H^{(2)}(\boldsymbol{k})]\upsilon_0 + \lambda_5 \sigma_z \upsilon_y + \epsilon \upsilon_z$. We have used the following parameters in the numerical calculations: $t_1 = 1$, $t_2 = 0.15$, $t_3 = 0.3$, $t_4 = 0.1$, $\lambda_1 = 1.5$, $\lambda_2 = 0.4$, $t_1' = 0.5$, $t_2' = 0.15$, $\lambda_1' = 0.7$, $\lambda_2' = 0.2$, $\lambda_3 = 0.2$, $\lambda_4 = 0.12$, $\lambda_5 = 0.05$, and $\epsilon = 0.05$.

APPENDIX B: TOPOLOGICAL CHARGE

The topological charges of a point node protected by $\widetilde{C}_{2z}^{\perp}$ and a line node protected by $\widetilde{M}_x^{\perp}$ can be determined as follows. First, for a point node, a zero-dimensional topological invariant Q is defined as

$$Q = \frac{1}{8}[N(k_N) - N(k_S)] \equiv \frac{1}{8}\Delta N \in \mathbb{Z}, \tag{B1}$$

where k_N (k_S) is the k_z momentum on the $\widetilde{C}_{2z}^{\perp}$ invariant axis slightly above (below) the Dirac point, and $N(k_z)$ is given by

$$\begin{aligned} N(k_z) &= N_+(k_z) - N_-(k_z), \\ N_{\pm}(k_z) &= N_{\pm}^c(k_z) - N_{\pm}^v(k_z), \end{aligned} \tag{B2}$$

where $N_{\pm}^c(k_z)$ and $N_{\pm}^v(k_z)$ denote the numbers of the conduction and valence bands with the $\widetilde{C}_{2z}^{\perp}$ eigenvalues of $\pm i$ at the momentum k_z. Let us note that the sum $N_+(k_z) + N_-(k_z)$ is constant on the $\widetilde{C}_{2z}^{\perp}$ invariant axis whereas the difference $N(k_z) = N_+(k_z) - N_-(k_z)$ can take an integer value, thus provides a topological index characterizing a Dirac point, which jumps across a Dirac point. The explicit form of the topological charge Q can be written as

$$\begin{aligned} Q &= \frac{1}{8}[(\Delta N_+^c - \Delta N_-^c) - (\Delta N_+^v - \Delta N_-^v)], \\ &= \frac{1}{4}(\Delta N_+^c - \Delta N_-^c), \\ &= -\frac{1}{4}(\Delta N_+^v - \Delta N_-^v), \end{aligned} \tag{B3}$$

which results from $\Delta N_+^c - \Delta N_-^c = -(\Delta N_+^v - \Delta N_-^v)$. Thus, to determine the topological charge Q, one can use either the change in the number of conduction bands $\Delta N_{\pm}^c$ or the change in the number of valence bands $\Delta N_{\pm}^v$.

There are several constraints on $N(k_z)$ imposed by the time-reversal and the inversion symmetries. Firstly, the antiunitary time-reversal symmetry, which commutes with the $\widetilde{C}_{2z}^{\perp}$ requires

$$N_{\pm}(k_z) = N_{\mp}(-k_z), \tag{B4}$$

thus

$$N(k_z) = -N(-k_z). \tag{B5}$$

On the other hand, the inversion symmetry anticommuting with $\widetilde{C}_{2z}^{\perp}$ requires

$$N_{\pm}(k_z) = N_{\mp}(-k_z), \tag{B6}$$

thus again

$$N(k_z) = -N(-k_z). \tag{B7}$$

The constraint in Eq. (B5) and Eq. (B7) naturally leads to the band structure and the corresponding distribution of $N(k_z)$ shown in Fig. 1.

In the case of a line node protected by $\widetilde{M}_x^{\perp}$, a zero-dimensional topological invariant Q' can be defined as follows. For a given gapless point $\boldsymbol{k}$ on a line node in the $k_x = \pi$ plane, one can find two points $\boldsymbol{k}_N$ and $\boldsymbol{k}_S$ in a way that the line connecting them is normal to the tangential vector at $\boldsymbol{k}$. Then the topological charge of a line node can be defined in the exactly the same way as in the case of the point node. Namely, a zero-dimensional topological invariant is defined as

$$Q' = \frac{1}{8}[N(\boldsymbol{k}_N) - N(\boldsymbol{k}_S)] \equiv \frac{1}{8}\Delta N \in \mathbb{Z}, \tag{B8}$$

where the definition of $N(\pi,k_y,k_z)$ is exactly the same as Eq. (B2). Namely,

$$\begin{aligned} N(\pi,k_y,k_z) &= N_+(\pi,k_y,k_z) - N_-(\pi,k_y,k_z), \\ N_{\pm}(\pi,k_y,k_z) &= N_{\pm}^c(\pi,k_y,k_z) - N_{\pm}^v(\pi,k_y,k_z), \end{aligned} \tag{B9}$$

where $N_{\pm}^c(\pi,k_y,k_z)$ and $N_{\pm}^v(\pi,k_y,k_z)$ denote the numbers of the conduction and valence bands with the $\widetilde{M}_x^{\perp}$ eigenvalues of $\pm i$ at the momentum (π,k_y,k_z). The topological invariant Q' measures the change in $N(\boldsymbol{k})$ across a line node in the $k_x = \pi$ plane.

There are several constraints on $N(\pi,k_y,k_z)$ imposed by the time-reversal and the inversion symmetries. Firstly, the antiunitary time-reversal symmetry, which commutes with the $\widetilde{M}_x^{\perp}$ requires

$$N_{\pm}(\pi,k_y,k_z) = N_{\mp}(\pi,-k_y,-k_z), \tag{B10}$$

thus

$$N(\pi,k_y,k_z) = -N(\pi,-k_y,-k_z). \tag{B11}$$

On the other hand, the inversion symmetry anticommuting with $\widetilde{M}_x^{\perp}$ requires

$$N_{\pm}(\pi,k_y,k_z) = N_{\mp}(\pi,-k_y,-k_z), \tag{B12}$$

thus again

$$N(\pi,k_y,k_z) = -N(\pi,-k_y-k_z). \tag{B13}$$

The constraint in Eqs. (B11) and (B13) naturally leads to the band structure and the corresponding distribution of $N(\pi,k_y,k_z)$ shown in Fig. 2.

It is worth to note that both time-reversal symmetry and inversion symmetry put the same constraint on the topological invariants as shown in Eqs. (B5) and (B7), and also in Eqs. (B11) and (B13). This means that as long as either P or T is preserved, the eigenstates always form pairs carrying quantized eigenvalues of $\widetilde{C}_{2z}^{\perp}$ or $\widetilde{M}_x^{\perp}$ in the relevant invariant space. Since an eigenstate at a generic momentum is nondegenerate when either T or P is broken, a pair is composed of nondegenerate states in this case. Hence whenever there is crossing of states having different eigenvalues of the relevant off-centered symmetries, Weyl point/line nodes with twofold degeneracy can be created.

APPENDIX C: CLIFFORD ALGEBRAS AND STABILITY OF NODAL POINTS AND NODAL LINES

Here we use Clifford algebras [50–56] to show the existence of stable Dirac points under $\widetilde{C}_{2z}^{\perp}$ and stable Dirac line nodes under $\widetilde{M}_x^{\perp}$, and determine the relevant topological charges. First, we show that stable Dirac points protected by $\widetilde{C}_{2z}^{\perp}$ can exist at the four TRIMs at $\boldsymbol{k} = (\pi,0,0)$, $(\pi,0,\pi)$, $(0,\pi,0)$, and $(0,\pi,\pi)$, where $\{P,\widetilde{C}_{2z}^{\perp}\} = 0$ and $(\widetilde{C}_{2z}^{\perp})^2 = -1$. Suppose that the effective Dirac Hamiltonian around a TRIM has a Dirac mass term γ_0,

$$H = q_x\gamma_x + q_y\gamma_y + q_z\gamma_z + m\gamma_0, \tag{C1}$$

where $\boldsymbol{q}$ is the momentum measured from the TRIM, m is the Dirac mass, and the gamma matrices mutually anticommute. The velocity is set equal to unity. We are going to see that the Dirac mass term $m\gamma_0$ is not allowed by symmetries.

Since T and P changes $\boldsymbol{q} \to -\boldsymbol{q}$, the invariance of the Dirac Hamiltonian requires the gamma matrices to obey

$$\{T,\gamma_x\} = \{T,\gamma_y\} = \{T,\gamma_z\} = [T,\gamma_0] = 0, \tag{C2}$$

$$\{P,\gamma_x\} = \{P,\gamma_y\} = \{P,\gamma_z\} = [P,\gamma_0] = 0. \tag{C3}$$

The symmetry operators T, P, and $\widetilde{C}_{2z}^{\perp}$ satisfy the following relations:

$$T^2 = -1, \qquad P^2 = 1, \qquad (\widetilde{C}_{2z}^{\perp})^2 = -1, \tag{C4}$$

$$[T,P] = [T,\widetilde{C}_{2z}^{\perp}] = \{P,\widetilde{C}_{2z}^{\perp}\} = 0. \tag{C5}$$

Since $\widetilde{C}_{2z}^{\perp}$ changes $q_{x,y} \to -q_{x,y}$, the invariance of the Hamiltonian under $\widetilde{C}_{2z}^{\perp}$ leads to the relations

$$\{\widetilde{C}_{2z}^{\perp},\gamma_x\} = \{\widetilde{C}_{2z}^{\perp},\gamma_y\} = [\widetilde{C}_{2z}^{\perp},\gamma_z] = [\widetilde{C}_{2z}^{\perp},\gamma_0] = 0. \tag{C6}$$

The Clifford algebra is constructed from the gamma matrices and the symmetry operators,

$$Cl_{4,4} = \{T, JT, J\gamma_0, \widetilde{C}_{2z}^{\perp}P\gamma_z; \gamma_x,\gamma_y,\gamma_z, P\gamma_x\gamma_y\gamma_z\}, \tag{C7}$$

where J represents the imaginary unit "i" satisfying $J^2 = -1$ and $\{T,J\} = 0$. Here we have used the notation for the Clifford algebra $Cl_{p,q} = \{e_1,\ldots,e_p;e_{p+1},\ldots,e_{p+q}\}$, where the generators e_j mutually anticommute and satisfy $e_j^2 = -1$ for $j = 1,\ldots,p$ and $e_j^2 = +1$ for $j = p+1,\ldots,p+q$. The existence/absence condition of the Dirac mass $m\gamma_0$ is determined by the extension problem [52]

$$Cl_{2,4} \to Cl_{3,4}. \tag{C8}$$

The relevant classifying space is $R_{2-4+2} = R_0$, and $\pi_0(R_0) = \mathbb{Z}$. This implies that no Dirac mass is available, and a Dirac point has a $\mathbb{Z}$ topological charge.

We have seen in Fig. 5(b) that Dirac point nodes are shifted from TRIMs in the eight-band model. Their stability can be understood with Clifford algebra as follows. We consider the Dirac Hamiltonian in Eq. (C1) with (q_x,q_y,q_z) measured from a Dirac point away from TRIMs. In this case T and P are not independent symmetries, and the product TP is the symmetry operator to be considered. It satisfies the relations

$$\begin{aligned}&(TP)^2 = -1,\\ &[TP,\gamma_x] = [TP,\gamma_y] = [TP,\gamma_z] = [TP,\gamma_0] = 0,\\ &\{TP,\widetilde{C}_{2z}^{\perp}\} = 0.\end{aligned} \tag{C9}$$

From he gamma matrices γ_μ and the symmetry operators, we can construct the Clifford algebra

$$Cl_{0,4} \otimes Cl_{2,1} = \{;\gamma_x,\gamma_y,\gamma_z,\gamma_0\} \otimes \{TP, JTP; \gamma_x\gamma_y\widetilde{C}_{2z}^{\perp}\}. \tag{C10}$$

The existence condition of the Dirac mass term $m\gamma_0$ is determined from the extension problem

$$Cl_{0,2} \otimes Cl_{2,1} \to Cl_{0,3} \otimes Cl_{2,1}, \tag{C11}$$

which is equivalent to the extension of complex Clifford algebra $Cl_4 \to Cl_5$, for which the relevant classifying space is $C_4 = C_0$. Since $\pi_0(C_0) = \mathbb{Z}$, no Dirac mass term is available, and a Dirac point has an integer topological index.

Next, we prove the stability of the line nodes protected by $\widetilde{M}_x^{\perp}$ in the $k_x = \pi$ plane where $\{P,\widetilde{M}_x^{\perp}\} = 0$ and $(\widetilde{M}_x^{\perp})^2 = -1$. We prove the stability of line nodes in two steps. First, we show that two bands touch at TRIMs with $k_x = \pi$. We consider the Dirac Hamiltonian

$$H = q_x\gamma_x + q_y\gamma_y + m\gamma_0, \tag{C12}$$

where (q_x,q_y) is a momentum measured from a TRIM with $k_z = 0$ or π. The gamma matrices satisfy the relations in Eqs. (C2) and (C3). The symmetry operators satisfy

$$\begin{aligned}&T^2 = -1, P^2 = 1, (\widetilde{M}_x^{\perp})^2 = -1,\\ &[T,P] = [T,\widetilde{M}_x^{\perp}] = \{P,\widetilde{M}_x^{\perp}\} = 0.\end{aligned} \tag{C13}$$

Since $\widetilde{M}_x^{\perp}$ changes the momentum $\boldsymbol{q} = (q_x,q_y,q_z) \to (-q_x,q_y,q_z)$, the commutation relations between gamma matrices and $\widetilde{M}_x^{\perp}$ are given by

$$\{\widetilde{M}_x^{\perp},\gamma_x\} = [\widetilde{M}_x^{\perp},\gamma_y] = [\widetilde{M}_x^{\perp},\gamma_0] = 0. \tag{C14}$$

Around TRIMs, T and P can be treated as symmetry operators. We can construct the Clifford algebra

$$Cl_{4,2} \otimes Cl_{1,0} = \{T, TJ, J\gamma_0, \widetilde{M}_x^{\perp}P\gamma_y; \gamma_x,\gamma_y\} \otimes \{P\gamma_x\gamma_y;\}. \tag{C15}$$

The existence condition of the Dirac mass term $m\gamma_0$ is determined by the extension problem

$$Cl_{2,2} \otimes Cl_{1,0} \to Cl_{3,2} \otimes Cl_{1,0}, \tag{C16}$$

or equivalently, $Cl_4 \to Cl_5$. The relevant classifying space is $C_4 = C_0$, and $\pi_0(C_0) = \mathbb{Z}$. Thus, no Dirac mass term is available. This means that the energy levels at these TRIMs are fourfold degenerate.

Next, we fix k_z to be constant different from 0 and π. We consider the Dirac Hamiltonian (C12), where q_x and q_y are now understood to be momentum measured from a line node on the constant k_z plane. Away from TRIMs, T and P are not independent symmetries, and instead the product TP is the symmetry operator to be considered. It obeys the relations

$$\begin{aligned}&(TP)^2 = -1,\\ &[TP,\gamma_x] = [TP,\gamma_y] = [TP,\gamma_0] = 0,\\ &\{TP,\widetilde{M}_x^{\perp}\} = 0.\end{aligned} \tag{C17}$$

Let us consider if the Dirac mass term $m\gamma_0$ is allowed in the Dirac Hamiltonian (C12) under the symmetries TP and $\widetilde{M}_x^{\perp}$. The Clifford algebra is constructed from the symmetry operators and the gamma matrices:

$$Cl_{1,3} \otimes Cl_{2,0} = \{J\gamma_x\widetilde{M}_x^{\perp};\gamma_x,\gamma_y,\gamma_0\} \otimes \{TP, JTP;\}. \tag{C18}$$

The extension problem $Cl_{1,1} \otimes Cl_{2,0} \to Cl_{1,2} \otimes Cl_{2,0}$ is equivalent to $Cl_{3,1} \to Cl_{4,1}$, which leads to the classifying space $R_{3+2-1} = R_4$; $\pi_0(R_4) = \mathbb{Z}$. This means that a line node is topologically stable on the $k_x = \pi$ plane.

APPENDIX D: LOW-ENERGY $\boldsymbol{k}\cdot\boldsymbol{p}$ HAMILTONIAN ANALYSIS

Here we construct the low-energy effective 4×4 Hamiltonian near the momentum $\boldsymbol{k} = (\pi,0,0)$ to understand the nature of nodal points/lines depending on the symmetry of the system. We take the following representation of symmetry operators:

$$\begin{aligned}&T = i\sigma_y\tau_z\mathcal{K}, P = -\tau_y, \widetilde{C}_{2z}^{\perp} = i\sigma_z\tau_z,\\ &\widetilde{M}_x^{\perp} = i\sigma_x\tau_z, \widetilde{M}_y^{\perp} = i\sigma_y.\end{aligned} \tag{D1}$$

The effective Hamiltonian can be obtained by collecting all symmetry-allowed operators up to linear order in $\boldsymbol{q} = \boldsymbol{k} - (\pi,0,0)$. In the following analysis we omit terms proportional to the unit 4×4 matrix for simplicity.

Firstly, the effective Hamiltonian invariant under T, P, and $\widetilde{C}_{2z}^{\perp}$ has the form

$$\begin{aligned}H_0 = {}& q_x(v_{1x}\tau_x + v_{2x}\sigma_x\tau_z + v_{3x}\sigma_y\tau_z)\\ &+ q_y(v_{1y}\tau_x + v_{2y}\sigma_x\tau_z + v_{3y}\sigma_y\tau_z)\\ &+ v_zq_z\sigma_z\tau_z\end{aligned} \tag{D2}$$

with energy eigenvalues $\pm E$ where

$$\begin{aligned}E^2 = {}& [(v_{1x}q_x + v_{1y}q_y)^2 + (v_{2x}q_x + v_{2y}q_y)^2\\ &+ (v_{3x}q_x + v_{3y}q_y)^2 + (v_zq_z)^2].\end{aligned} \tag{D3}$$

There is a Dirac point at $\boldsymbol{q} = 0$.

Secondly, the effective Hamiltonian invariant under T, P, and $\widetilde{M}_x^{\perp}$ has the form

$$H_0 = q_x(v_{1x}\tau_x + v_{2x}\sigma_y\tau_z + v_{3x}\sigma_z\tau_z) + (v_yq_y + v_zq_z)\sigma_x\tau_z, \tag{D4}$$

whose energy eigenvalues are

$$E = \pm\left[\left(v_{1x}^2 + v_{2x}^2 + v_{3x}^2\right)q_x^2 + (v_yq_y + v_zq_z)^2\right]^{1/2}. \tag{D5}$$

There is a Dirac line node located at $q_x = 0$ and $v_y q_y + v_z q_z = 0$.

Finally, the effective Hamiltonian invariant under T, P, $\widetilde{C}_{2z}^{\perp}$, and $\widetilde{M}_x^{\perp}$ has the form

$$H_0 = q_x(v_{1x}\tau_x + v_{2x}\sigma_y\tau_z) + v_y q_y \sigma_x \tau_z, \tag{D6}$$

whose energy eigenvalues are

$$E = \pm\left[\left(v_{1x}^2 + v_{2x}^2\right)q_x^2 + (v_y q_y)^2\right]^{1/2}. \tag{D7}$$

There is a Dirac line located at $q_x = q_y = 0$. In all three cases, the influence of external magnetic field can be examined by adding a Zeeman term $\boldsymbol{H}\cdot\boldsymbol{\sigma} = h_x\sigma_x + h_y\sigma_y + h_z\sigma_z$ to H_0, and the results of the analysis are summarized in Table I.

APPENDIX E: SINGLE DIRAC POINT/LINE NODE PROTECTED BY OFF-CENTERED SCREW/GLIDE SYMMETRIES

Let us first consider an off-centered screw rotation $\widetilde{C}_{2z}^{\parallel,\perp} = \{C_{2z}|\frac{1}{2}\hat{x} + \frac{1}{2}\hat{z}\}$ which transforms the spatial coordinate as

$$\widetilde{C}_{2z}^{\parallel,\perp} : (x,y,z) \to \left(-x + \frac{1}{2}, -y, z + \frac{1}{2}\right). \tag{E1}$$

Let us note that the partial translation in $\widetilde{C}_{2z}^{\parallel,\perp}$ has both the parallel and perpendicular components relative to the rotation axis. The eigenvalues of $\widetilde{C}_{2z}^{\parallel,\perp}$ are given by $c_{\pm}(k_z) = \pm i e^{i\frac{1}{2}k_z}$, which is momentum dependent. After straightforward calculation, one can find the following commutation relations:

$$\widetilde{C}_{2z}^{\parallel,\perp} PT = e^{-ik_x + ik_z} PT \widetilde{C}_{2z}^{\parallel,\perp},$$
$$\widetilde{C}_{2z}^{\parallel,\perp} P = e^{ik_x - ik_z} P \widetilde{C}_{2z}^{\parallel,\perp}. \tag{E2}$$

Thus, along the $\widetilde{C}_{2z}^{\parallel,\perp}$ invariant lines with $k_x = \pi$, we find

$$\widetilde{C}_{2z}^{\parallel,\perp}[PT|c_{\pm}(k_z)\rangle] = c_{\pm}(k_z)[PT|c_{\pm}(k_z)\rangle], \tag{E3}$$

where $\widetilde{C}_{2z}^{\parallel,\perp}|c_{\pm}(k_z)\rangle = c_{\pm}(k_z)|c_{\pm}(k_z)\rangle$. Namely, the Kramers degenerate states related by PT at a momentum $\boldsymbol{k}$ have the same $\widetilde{C}_{2z}^{\parallel,\perp}$ eigenvalues $c_{\pm}(k_z) = \pm i e^{i\frac{1}{2}k_z}$. From $c_{\pm}(k_z + 2\pi) = c_{\mp}(k_z)$, one can see that two sets of degenerate bands having different $\widetilde{C}_{2z}^{\parallel,\perp}$ eigenvalues should be interchanged when k_z is shifted by 2π. Also, the fact that $c_{\pm}(k_z)$ is pure imaginary (real) when $k_z = 0$ ($k_z = \pi$) indicates that the two bands should be degenerate at $k_z = 0$ to satisfy time-reversal symmetry. This consideration naturally leads to the band structure shown in Figs. 9(a)–9(c) where two sets of degenerate bands having different $\widetilde{C}_{2z}^{\parallel,\perp}$ eigenvalues form a doublet pair with a single Dirac-type crossing at $k_z = 0$. This doublet with a single Dirac point provides a basic building block to construct the band structure along the $\widetilde{C}_{2z}^{\parallel,\perp}$ invariant lines with $k_x = \pi$.

Now we consider an off-centered glide mirror $\widetilde{M}_z^{\parallel,\perp} = \{M_z|\frac{1}{2}\hat{x} + \frac{1}{2}\hat{z}\}$, which transforms the spatial coordinate as

$$\widetilde{M}_z^{\parallel,\perp} : (x,y,z) \to \left(x + \frac{1}{2}, y, -z + \frac{1}{2}\right). \tag{E4}$$

Let us note that the partial translation in $\widetilde{M}_z^{\parallel,\perp}$ has both the parallel and perpendicular components relative to the mirror plane. The eigenvalues of $\widetilde{M}_z^{\parallel,\perp}$ are given by $m_{\pm}(k_x,k_y) = \pm i e^{i\frac{1}{2}k_x}$, which is momentum dependent. After straightforward calculation, one can find the following commutation relations

$$\widetilde{M}_z^{\parallel,\perp} PT = e^{-ik_z + ik_x} PT \widetilde{M}_z^{\parallel,\perp},$$
$$\widetilde{M}_z^{\parallel,\perp} P = e^{ik_z - ik_x} P \widetilde{M}_z^{\parallel,\perp}. \tag{E5}$$

Thus, in the $k_z = \pi$ plane, we find

$$\widetilde{M}_z^{\parallel,\perp}[PT|m_{\pm}(k_x,k_y)\rangle] = m_{\pm}(k_x,k_y)[PT|m_{\pm}(k_x,k_y)\rangle], \tag{E6}$$

where $\widetilde{M}_z^{\parallel,\perp}|m_{\pm}(k_x,k_y)\rangle = m_{\pm}(k_x,k_y)|m_{\pm}(k_x,k_y)\rangle$. Namely, the degenerate states related by PT at a momentum $\boldsymbol{k}$ have the same $\widetilde{M}_z^{\parallel,\perp}$ eigenvalues $m_{\pm}(k_x,k_y) = \pm i e^{i\frac{1}{2}k_x}$. From $m_{\pm}(k_x + 2\pi,k_y) = m_{\mp}(k_x,k_y)$, one can see that two sets of degenerate bands having different $\widetilde{M}_z^{\parallel,\perp}$ eigenvalues should be interchanged when k_x is shifted by 2π. Also, the fact that $m_{\pm}(k_x,k_y)$ is pure imaginary when $(k_x,k_y) = (0,0), (0,\pi)$ indicates that the two bands should be degenerate at these two points to satisfy time-reversal symmetry. This consideration naturally leads to the band structure shown in Figs. 9(d)–9(f) where two sets of degenerate bands having different $\widetilde{M}_z^{\parallel,\perp}$ eigenvalues form a doublet pair in the whole $k_z = \pi$ plane with a single open-shaped Dirac line node passing $(k_x,k_y) = (0,0)$ and $(0,\pi)$. This doublet with a single Dirac line node provides a basic building block to construct the band structure in the $k_z = \pi$ plane.

[1] A. H. Castro Neto, F. Guinea, N. M. R. Peres, K. S. Novoselov, and A. K. Geim, The electronic properties of graphene, Rev. Mod. Phys. **81**, 109 (2009).

[2] Y. Kim, B. J. Wieder, C. L. Kane, and A. M. Rappe, Dirac Line Nodes in Inversion Symmetric Crystals, Phys. Rev. Lett. **115**, 036806 (2015).

[3] H. Weng, Y. Liang, Q. Xu, R. Yu, Z. Fang, X. Dai, and Y. Kawazoe, Topological node-line semimetal in three-dimensional graphene network, Phys. Rev. B **92**, 045108 (2015).

[4] R. Yu, H. Weng, Z. Fang, X. Dai, and X. Hu, Topological Node-Line Semimetal and Dirac Semimetal State in Antiperovskite Cu_3PdN, Phys. Rev. Lett. **115**, 036807 (2015).

[5] G. P. Mikitik, and Yu. V. Sharlai, Band-contact lines in the electron energy spectrum of graphite, Phys. Rev. B **73**, 235112 (2006).

[6] K. Mullen, B. Uchoa, and D. T. Glatzhofer, Line of Dirac Nodes in Hyperhoneycomb Lattices, Phys. Rev. Lett. **115**, 026403 (2015).

[7] H. Huang, J. Liu, D. Vanderbilt, and W. Duan, Topological nodal-line semimetals in alkaline-earth stannides, germanides, and silicides, Phys. Rev. B **93**, 201114(R) (2016).

[8] M. Ezawa, Loop-Nodal and Point-Nodal Semimetals in Three-Dimensional Honeycomb Lattices, Phys. Rev. Lett. **116**, 127202 (2016).

[9] H. Hirayama, R. Okugawa, T. Miyake, and S. Murakami, Topological Dirac nodal lines and surface charges in fcc alkaline earth metals, Nat. Commun. **8**, 14022 (2017).

[10] T. T. Heikkila and G. E. Volovik, Nexus and Dirac lines in topological materials, New J. Phys. **17**, 093019 (2015).

[11] C.-K. Chiu and A. P. Schnyder, Classification of reflection-symmetry-protected topological semimetals and nodal superconductors, Phys. Rev. B **90**, 205136 (2014).

[12] L. S. Xie, L. M. Schoop, E. M. Seibel, Q. D. Gibson, W. Xie, and R. J. Cava, A new form of Ca_3P_2 with a ring of Dirac nodes, APL Mat. **3**, 083602 (2015).

[13] M. Zheng, C. Fang, G. Chang, Y.-A. Chen, T. Hsieh, A. Bansil, H. Lin, and L. Fu, Topological semimetals and topological insulators in rare earth monopnictides, arXiv:1504.03492.

[14] Z. Gao, M. Hua, H. Zhang, and X. Zhang, Classification of stable Dirac and Weyl semimetals with reflection and rotational symmetry, Phys. Rev. B **93**, 205109 (2016).

[15] A. Yamakage, Y. Yamakawa, Y. Tanaka, and Y. Okamoto, Line-node dirac semimetal and topological insulating phase in noncentrosymmetric pnictides CaAgX (X = P, As), J. Phys. Soc. Jpn. **85**, 013708 (2016).

[16] T. Hyart and T. T. Heikkila, Momentum-space structure of surface states in a topological semimetal with a nexus point of Dirac lines, Phys. Rev. B **93**, 235147 (2016).

[17] Y. Chen, Y.-M. Lu, and H. Y. Kee, Topological crystalline metal in orthorhombic perovskite iridates, Nat. Commun. **6**, 6593 (2015).

[18] G. Bian, T.-R. Chang, R. Sankar, S.-Y. Xu, H. Zheng, T. Neupert, C.-K. Chiu, S.-M. Huang, G. Chang, I. Belopolski, D. S. Sanchez, M. Neupane, N. Alidoust, C. Liu, B. Wang, C.-C. Lee, H.-T. Jeng, A. Bansil, F. Chou, H. Lin, and M. Z. Hasan, Topological nodal-line fermions in the non-centrosymmetric superconductor compound $PbTaSe_2$, Nat. Commun. **7**, 10556 (2016).

[19] G. Bian, T.-R. Chang, H. Zheng, S. Velury, S.-Y. Xu, T. Neupert, C.-K. Chiu, S.-M. Huang, D. S. Sanchez, I. Belopolski, N. Alidoust, P.-J. Chen, G. Chang, A. Bansil, H.-T. Jeng, H. Lin, and M. Z. Hasan, Drumhead surface states and topological nodal-line fermions in $TlTaSe_2$, Phys. Rev. B **93**, 121113(R) (2016).

[20] S. M. Young, S. Zaheer, J. C. Y. Teo, C. L. Kane, E. J. Mele, and A. M. Rappe, Dirac Semimetal in Three Dimensions, Phys. Rev. Lett. **108**, 140405 (2012).

[21] J. A. Steinberg, S. M. Young, S. Zaheer, C. L. Kane, E. J. Mele, and A. M. Rappe, Bulk Dirac Points in Distorted Spinels, Phys. Rev. Lett. **112**, 036403 (2014).

[22] Z. Wang, Y. Sun, X. Q. Chen, C. Franchini, G. Xu, H. Weng, X. Dai, and Z. Fang, Dirac semimetal and topological phase transitions in A_3Bi (A=Na, K, Rb), Phys. Rev. B **85**, 195320 (2012).

[23] Z. Wang, H. Weng, Q. Wu, X. Dai, and Z. Fang, Three-dimensional Dirac semimetal and quantum transport in Cd_3As_2, Phys. Rev. B **88**, 125427 (2013).

[24] B.-J. Yang and N. Nagaosa, Classification of stable three-dimensional Dirac semimetals with nontrivial topology, Nat. Commun. **5**, 4898 (2014).

[25] B.-J. Yang, T. Morimoto, and A. Furusaki, Topological charges of three-dimensional Dirac semimetals with rotation symmetry, Phys. Rev. B **92**, 165120 (2015).

[26] C. Fang, H. Weng, X. Dai, and Z. Fang, Topological nodal line semimetals, Chin. Phys. B **25**, 117106 (2016).

[27] Z. K. Liu, B. Zhou, Y. Zhang, Z. J. Wang, H. M. Weng, D. Prabhakaran, S.-K. Mo, Z. X. Shen, Z. Fang, X. Dai, Z. Hussain, and Y. L. Chen, Discovery of a three-dimensional topological Dirac semimetal, Na_3Bi, Science **343**, 864 (2014).

[28] S.-Y. Xu, C. Liu, S. K. Kushwaha, T.-R. Chang, J. W. Krizan, R. Sankar, C. M. Polley, J. Adell, T. Balasubramanian, K. Miyamoto, N. Alidoust, G. Bian, M. Neupane, I. Belopolski, H.-T. Jeng, C.-Y. Huang, W.-F. Tsai, H. Lin, F. C. Chou, T. Okuda, A. Bansil, R. J. Cava, and M. Z. Hasan, Observation of a bulk 3D Dirac multiplet, Lifshitz transition, and nestled spin states in Na_3Bi, arXiv:1312.7624.

[29] M. Neupane, S.-Y. Xu, R. Sankar, N. Alidoust, G. Bian, C. Liu, I. Belopolski, T.-R. Chang, H.-T. Jeng, H. Lin, A. Bansil, F. Chou, and M. Z. Hasan, Observation of a three dimensional topological Dirac semimetal phase in high-mobility Cd_3As_2, Nat. Commun. **5**, 3786 (2014).

[30] S. Borisenko, Q. Gibson, D. Evtushinsky, V. Zabolotnyy, B. Büchner, and R. J. Cava, Experimental Realization of a Three-Dimensional Dirac Semimetal, Phys. Rev. Lett. **113**, 027603 (2014).

[31] S. Jeon, B. B. Zhou, A. Gyenis, B. E. Feldman, I. Kimchi, A. C. Potter, Q. D. Gibson, R. J. Cava, A. Vishwanath, and A. Y azdani, Landau quantization and quasiparticle interference in the three-dimensional Dirac semimetal Cd_3As_2, Nat. Mater. **13**, 851 (2014).

[32] Z. K. Liu, J. Jiang, B. Zhou, Z. J. Wang, Y. Zhang, H. M. Weng, D. Prabhakaran, S.-K. Mo, H. Peng, P. Dudin, T. Kim, M. Hoesch, Z. Fang, X. Dai, Z. X. Shen, D. L. Feng, Z. Hussain, and Y. L. Chen, A stable three-dimensional topological Dirac semimetal Cd_3As_2, Nat. Mater. **13**, 677 (2014).

[33] C. J. Bradley and A. P. Cracknell, *The Mathematical Theory of Symmetry in Solids* (Clarendon Press, Oxford, 1972).

[34] S. M. Young and C. L. Kane, Dirac Semimetals in two Dimensions, Phys. Rev. Lett. **115**, 126803 (2015).

[35] A. A. Burkov, M. D. Hook, and L. Balents, Topological nodal semimetals, Phys. Rev. B **84**, 235126 (2011).

[36] M. Phillips, and V. Aji, Tunable line node semimetals, Phys. Rev. B **90**, 115111 (2014).

[37] T. L. Hughes, E. Prodan, and B. A. Bernevig, Inversion-symmetric topological insulators, Phys. Rev. B **83**, 245132 (2011).

[38] A. M. Turner, Y. Zhang, R. S. K. Mong, and A. Vishwanath, Quantized response and topology of magnetic insulators with inversion symmetry, Phys. Rev. B **85**, 165120 (2012).

[39] D. Vanderbilt and R. D. King-Smith, Electric polarization as a bulk quantity and its relation to surface charge, Phys. Rev. B **48**, 4442 (1993).

[40] Y.-H. Chan, C.-K. Chiu, M. Y. Chou, and A. P. Schnyder, Topological semimetals with line nodes and drumhead surface states, Phys. Rev. B **93**, 205132 (2016).

[41] C. Fang, Y. Chen, H. Y. Kee, and L. Fu, Topological nodal line semimetals with and without spin-orbital coupling, Phys. Rev. B **92**, 081201(R) (2015).

[42] Y. Chen, H.-S. Kim, and H. Y. Kee, Topological crystalline semimetals in non-symmorphic lattices, Phys. Rev. B **93**, 155140 (2016).

[43] H. Watanabe, H. C. Po, M. P. Zaletel, and A. Vishwanath, Filling-Enforced Gaplessness in Band Structures of the 230 Space Groups, Phys. Rev. Lett. **117**, 096404 (2016).

[44] J. Liu, D. Kriegner, L. Horak, D. Puggioni, C. Rayan Serrao, R. Chen, D. Yi, C. Frontera, V. Holy, A. Vishwanath, J. M. Rondinelli, X. Marti, and R. Ramesh, Strain-induced nonsymmorphic symmetry breaking and removal of Dirac semimetallic nodal line in an orthoperovskite iridate, Phys. Rev. B **93**, 085118 (2016).

[45] Q.-F. Liang, J. Zhou, R. Yu, Z. Wang, and H. Weng, Node-surface and node-line fermions from nonsymmorphic lattice symmetries, Phys. Rev. B **93**, 085427 (2016).

[46] B. J. Wieder and C. L. Kane, Spin-orbit semimetals in the layer groups, Phys. Rev. B **94**, 155108 (2016).

[47] P. Goswami and S. Chakravarty, Quantum Criticality Between Topological and Band Insulators in 3+1 Dimensions, Phys. Rev. Lett. **107**, 196803 (2011).

[48] Y. Huh, E.-G. Moon, and Y. B. Kim, Long range Coulomb interaction in nodal ring semimetals, Phys. Rev. B **93**, 035138 (2016).

[49] W. M. H. Natori, E. C. Andrade, E. Miranda, and R. G. Pereira, Chiral Spin-Orbital Liquids with Nodal Lines, Phys. Rev. Lett. **117**, 017204 (2016).

[50] A. Kitaev, Periodic table for topological insulators and superconductors, AIP Conf. Proc. **1134**, 22 (2009).

[51] T. Morimoto and A. Furusaki, Topological classification with additional symmetries from Clifford algebras, Phys. Rev. B **88**, 125129 (2013).

[52] T. Morimoto and A. Furusaki, Weyl and Dirac semimetals with Z_2 topological charge, Phys. Rev. B **89**, 235127 (2014).

[53] Y. X. Zhao and Z. D. Wang, Topological Classification and Stability of Fermi Surfaces, Phys. Rev. Lett. **110**, 240404 (2013).

[54] Y. X. Zhao and Z. D. Wang, Topological connection between the stability of Fermi surfaces and topological insulators and superconductors, Phys. Rev. B **89**, 075111 (2014).

[55] K. Shiozaki and M. Sato, Topology of crystalline insulators and superconductors, Phys. Rev. B **90**, 165114 (2014).

[56] K. Shiozaki, M. Sato, and K. Gomi, Topology of nonsymmorphic crystalline insulators and superconductors, Phys. Rev. B **93**, 195413 (2016).